Temperature sensitivity of bat antibodies links metabolic state with antigen-recognition diversity

Nia Toshkova[1#], Violeta Zhelyzkova[1,2#], Alejandra Reyes-Ruiz[2], Eline Haerens[2], Marina de Castro Deus[2], Robin V. Lacombe[2], Maxime Lecerf[2], Gaelle Gonzalez[3], Nolwenn Jouvenet[4], Cyril Planchais[5], and Jordan D. Dimitrov[2*]

[1]National Museum of Natural History, Bulgarian Academy of Sciences, 1000 Sofia, Bulgaria

[2]Centre de Recherche des Cordeliers, INSERM, CNRS, Sorbonne Université, Université Paris Cité, 75006 Paris, France

[3]ANSES, INRAE, Ecole Nationale Vétérinaire d'Alfort, UMR Virologie, Laboratoire de Santé Animale, 94700, Maisons-Alfort, France

[4] Institut Pasteur, Université de Paris Cité, CNRS UMR3569, Virus Sensing and Signaling Unit, 75015 Paris, France.

[5]Institut Pasteur, INSERM U1222, Université Paris Cité, Humoral Immunology Unit, 75015 Paris, France

[#]These authors contributed equally to this work

Running title: Temperature diversifies bat antibodies

[*]**Corresponding author**
Jordan D. Dimitrov,
INSERM UMRS 1138,
Centre de Recherche des Cordeliers, 75006 Paris, France.
Tel: +33 1-44278206;
E-mail: jordan.dimitrov@sorbonne-universite.fr

Abstract

Bat immune system features multiple unique properties such as dampened inflammatory responses and increased tissue protection, explaining their long lifespan and tolerance to viral infections. Here, we demonstrated that body temperature fluctuations corresponding to different physiological states in bats exert a dramatic impact on their antibody repertoires. At elevated temperatures typical for flight, IgG from *Myotis myotis* and *Nyctalus noctula* showed elevated antigen binding strength and diversity, recognizing both pathogen-derived antigens and autoantigens. The opposite was observed at temperatures reflecting inactive physiological states. This behavior was not observed for IgG antibodies of human and other mammals, or antibodies of birds. Importantly, diversification of bat antibody specificities resulted in preferential recognition of damaged endothelial and epithelial cells, indicating an anti-inflammatory function. The temperature-sensitivity of bat antibodies was mediated by the variable regions of immunoglobulin molecules. Additionally, we revealed specific molecular features of bat IgG such as low thermodynamic stability and implication of hydrophobic interactions in antigen binding as well as high prevalence of polyreactivity. Overall, our results extend the understanding of bat tolerance to disease and inflammation and highlight the link between metabolism and immunity. This might have important repercussions for human health in the future.

Keywords:

Antibodies; Bats; Immune diversity; Bat immunology; Antigen binding; Body temperature; Metabolism; Disease tolerance; Immune homeostasis; Oxidative stress.

Introduction

Bats (order *Chiroptera*) represent the second largest order of mammals, after rodents, numbering more than 1400 species. They are the only mammals capable of powered flight and possess several exceptional physiological characteristics such as long lifespan, low incidence of age-related diseases, and elevated tolerance to viral infections [1]. Different bat species have been reported to harbor a particularly high diversity of viruses [2-6], some of which can cause severe diseases in humans [7]. Yet, they rarely succumb to immunopathology, thanks to some unique evolutionary adaptations of essential immune pathways [1,7-9]. For instance, bats feature a particular genetic and functional organization of the interferon (IFN) system that can manifest in constitutive tissue expression of IFNs, differential expression of IFN-stimulated genes, and altered kinetics of IFN responses [10,11]. Additionally, in contrast to primates and rodents, many bat species demonstrate impairments in the detection and response to damage-associate patterns (DAMPs), such as cytosolic DNA [12-15].

In addition to the genetic features of their immune components, physiological peculiarities of bats may also play a significant role in tolerance to viral infections. In particular, body temperature in bats can significantly fluctuate on a seasonal and quotidian basis, especially in temperate regions. During the metabolically demanding flight, it is usually around 40 °C, reaching up to 42 °C in some species [16], however, it can drop to ≈20 °C during shallow torpor [17] and even below <10 °C during hibernation [18,19]. Consequently, both high and low body temperatures have been proposed as mechanisms to control infection by providing suboptimal conditions for pathogen replication. In detail, the rise in temperature during flight creates a similar physiological condition as the febrile response in other mammals (so called "flight-as-fever" hypothesis), which is recognized as an evolutionary ancient immune defense mechanism [16,20]. On the other hand, even short torpor bouts have been shown to reduce viral growth rate sufficiently to control infection [17]. Yet, how temperature fluctuations affect the innate and

81 adaptive immune compartments of bats and how this can contribute to increased pathogen
82 tolerance is barely known.

83 In the present work, we aimed to fill this gap by rationally planning experiments based on the
84 specific life history traits and physiological characteristics of bats. In particular, we
85 concentrated on antibodies as the major component of the humoral immune response with
86 central roles in adaptive immune defense against pathogens and maintenance of immune
87 homeostasis [21]. Our data revealed an unconventional mechanism for diversification of immune
88 specificity of IgG antibodies driven by temperature in two bat species, the Greater moused-
89 eared bat (*Myotis myotis,* Borkhausen, 1797) and the Common noctule (*Nyctalus noctula,*
90 Schreber, 1774). Additionally, we describe unique physicochemical features of bat antibodies
91 that might explain temperature sensitivity. Finally, we identified potential immune defense,
92 homeostatic, and anti-inflammatory functions of this phenomenon that contribute to better
93 understand the mechanisms of the elevated disease tolerance in bats.

94

95 **Results**

96 **Temperature modulates the antigen-binding function of bat IgG antibodies**

97 As a consequence of their specific diurnal and seasonal cycles, bats experience large
98 fluctuations in body temperature, and so does their immune system [9,16,18,19,22-26]. This might be
99 particularly relevant to antibodies as they rely on molecular recognition to provide antigen
100 specificity, a process that is strongly affected by a variety of physicochemical factors. Thus, we
101 investigated antigen-binding properties of bat antibodies at three different temperatures: 4, 22
102 and 42 °C, reflecting physiological states of hibernation, shallow torpor, and active flight,
103 respectively. To this end, we purified total IgG from sera of two bat species, *M. myotis* and *N.*
104 *noctula*, as well as from healthy humans and 4 other mammal species. Next, we analyzed

105 antibody binding as a function of temperature to panels of unrelated mammalian and pathogen-
106 derived proteins and LPS using high-throughput ELISA (Fig. 1a and Supplementary Fig. 1 and.
107 2). The results revealed only negligible reactivity of polyclonal IgG from both bat species to
108 studied antigens at 4 and 22 °C. However, the same IgG samples demonstrated significant
109 broadening of their antigen recognition potential at 42 °C (Fig. 1a and Supplementary Fig. 1
110 and 2). At high temperature, bat antibodies augmented their reactivity to almost all antigens in
111 the panel, yet four proteins were identified as preferentially recognized outliers: NS1 protein
112 of tick-borne encephalitis virus (TBEV), rabies virus glycoprotein, measles virus
113 hemagglutinin, and thyroglobulin (Fig. 1a and Supplementary Fig. 1b). In contrast, immune
114 specificity of human IgG, either pooled or from individual donors, was not significantly
115 affected by temperature (Fig. 1a and Supplementary Fig. 1b), whereby it demonstrated
116 significant (and independent from temperature within the range of 4 – 42 °C) binding to LysM
117 (*E. faecalis*), LPS (*E. coli*), SARS-CoV-2 Spike (S) protein, and influenza virus haemagglutinin
118 (HA) (Fig. 1a and Supplementary Fig. 1a and Fig. 2). Notably, at 42 °C, human IgG
119 demonstrated a tendency for reduced binding to LPS. Similarly, temperature did not affect (or
120 affected only negligibly) the binding of IgG purified from sera of other mammalian species –
121 mouse, rabbit, goat, and cattle (Supplementary Fig. 2), or the binding of IgY from four bird
122 species (Supplementary Fig. 3). Notably, birds, much like bats have been reported to increase
123 their metabolic rates and heat production during flight [27].

124 Next, we applied surface plasmon resonance to quantify the effect of temperature on antigen-
125 binding properties of bat antibodies. We assessed antibody binding to the two antigens
126 recognized with the highest intensity in the previous ELISA experiment: NS1 protein of TBEV
127 and rabies virus glycoprotein (Fig. 1b). The real-time kinetic analysis demonstrated that
128 binding of IgG from *M. myotis* to both proteins progressively increased as a function of
129 temperature. At temperatures within the range of 4 – 16 °C, binding was barely detectable even

130 at the highest antibody concentrations. In contrast, at the highest temperature achievable with
131 the instrument (40 °C), interaction of bat IgG was considerable and subjectable to global kinetic
132 analysis (Supplementary Fig. 4). These showed that bat IgG bound to NS1 protein and rabies
133 virus glycoprotein with physiologically relevant values of apparent binding affinity (K_D values
134 of 26 and 189 nM, respectively; Fig. 1b and Supplementary Fig. 4).

135 To understand whether reactivity of bat antibodies is still affected by temperature in a complex
136 biological system, we also performed ELISA experiments using whole sera (Fig. 1c). Again,
137 binding of bat IgG to NS1 of TBEV and rabies virus glycoprotein profoundly increased with
138 temperature, in contrast to binding of human IgG to SARS-CoV-2 S protein and influenza virus
139 HA. (Fig. 1a). These results were in complete agreement with our previous findings obtained
140 with purified IgG. However, we noted that reactivity of bat antibodies to the blocking agent
141 was elevated in complete sera as compared to purified IgG (Supplementary. Fig. 5). This could
142 be explained by the possible binding of immunoglobulin classes other than IgG present in
143 complete sera.

144 To further confirm that temperature sensitivity of bat antibodies is a species-specific and not
145 an individual trait, we used 12 additional serum pools from *M. myotis* to test IgG binding to
146 NS1 of TBEV. As expected, at temperature typical for high metabolic rate (42 °C), there was a
147 marked increase in IgG binding to the antigen (Supplementary. Fig. 6a). Importantly, the
148 phenomenon was observed in sera collected both before and after hibernation (Supplementary.
149 Fig. 6b), a period associated with a significant suppression of immune functions and a decrease
150 in antibody production [28] .

151 Finally, using immunofluorescence, we elucidated reactivity of bat IgG to HEp-2 cells, which
152 are human cells traditionally used to detect the presence of autoantibodies. Our results indicated
153 only negligible binding of both human and bat (*M. myotis*) IgG to HEp-2 at 22 °C, with bat
154 antibodies demonstrating higher reactivity (Fig. 1d). However, at 42 °C, bat antibodies

155 markedly increased their binding to different cellular structures, both cytosolic and nuclear, a
156 typical characteristic of autoantibodies (Fig. 1d); this was not observed with human IgG. In
157 addition, elevated temperature significantly increased the reactivity to HEp-2 cells of IgG
158 purified from three other bat species: *Nyctalus noctula, Myotis blythii* (Lasser mouse-eared
159 bat), and *Myotis capaccinii* (Long-fingered bat) (Supplementary. Fig. 7).

160 Collectively, these results show that bat IgG (purified or in whole sera) considerably increases
161 its antigen-binding reactivity towards pathogen-derived and mammalian antigens at
162 temperatures typical for high metabolic rate (observed during flight). Conversely, a raise in
163 temperature does not change the reactivity of antibodies from human, other mammals, as well
164 as birds.

165

166 **Temperature broadens diversity of bat antibody antigen specificities**

167 In order to obtain more integrative insights about the effect of temperature on bat (and human)
168 antibody repertoires, we applied protein array technology. Human proteome arrays HuProt™
169 display >17 000 different proteins, thus allowing the study of immune reactivity to a huge
170 diversity of targets with different sequences and structural features. In accordance with the
171 previous results (Figure 1), our pool of purified IgG from *M. myotis* manifested only negligible
172 binding to protein targets at 22 °C. However, when the same pool was probed at 42 °C, we
173 observed a marked broadening in the repertoire of recognized proteins (Fig. 2a). At elevated
174 temperatures, bat IgG recognized a significant fraction of tested proteins (>2400 or ≈ 14 % of
175 all proteins) with a high binding intensity (MFI > 1000), whereby only 19 proteins were
176 recognized with a high binding intensity at 22 °C. In contrast, temperature affected binding
177 diversity of human IgG to a considerably lower extent (Fig. 2a). At 42 °C, human antibodies
178 recognized 134 proteins with a high binding intensity – a more limited increase in antigen-

179 binding diversity as compared to 22 °C where human antibodies interacted strongly with 8
180 proteins (Fig. 2a). The considerable difference in the diversity of bat and human immune
181 specificities is particularly obvious when plotted together (Fig. 2b): even though at 22 °C bat
182 antibodies displayed slightly elevated immune reactivity as compared to human, at 42 °C a
183 considerable asymmetry in the protein binding landscape was evident (Fig. 2b). Finally, the
184 plots of Z-scores indicated that at high temperature, a larger set of proteins was recognized with
185 significantly higher than average binding intensity by bat IgG as compared to human IgG (Fig.
186 2c). Similar results were obtained from *N. noctula* where antigen binding diversity of pooled
187 IgG also considerably increased at 42 °C as compared to 22 °C (Supplementary. Fig. 8).

188 These data indicate that bat antibodies can significantly broaden their antigen binding diversity
189 at temperatures typical for active metabolic state. On the contrary, antigen binding diversity of
190 human antibody repertoire is much less affected by temperature variation.

191

192 **Temperature differentially affects Fab- and Fc-dependent interactions of bat antibodies**

193 Next, we performed experiments to rule out possible non-specific effects of temperature on bat
194 IgG molecules. First, our aim was to establish if other bat proteins change their specificity as a
195 function of temperature. Thus, binding of serum albumin purified from *M. myotis* to the
196 proteins available in a crude extract of *M. myotis* epithelial cells was not affected by an increase
197 in temperature, contrary to the behavior of IgG purified from the same serum pool
198 (Supplementary. Fig. 9). With this experiment we showed that the broadened reactivity as a
199 function of temperature is not typical for all bat proteins.

200 To demonstrate further that temperature specifically affects the antigen-binding region of bat
201 antibodies, we generated $F(ab')_2$ fragments from bat IgG by enzymatic digestion with the

202 bacterial protease IdeS (Fig. 3a). As with whole IgG, binding of bat $F(ab')_2$ to distinct antigens
203 strongly increased as a function of temperature (Fig. 3b).

204 Next, we focused on the effect of temperature on interactions mediated by the Fc portion of
205 IgG molecules. Comparison of sequences of the constant portions of IgG1 of *M. myotis* and
206 human showed relatively high degree of homology (ca. 67 %, Supplementary Fig. 10). It is
207 noteworthy that the identity of this region between *M. myotis* and murine IgG subclasses was
208 lower (ca. 58 % for murine IgG2b, Supplementary Fig. 10). The high sequence identity of their
209 constant portions can explain the potential of human Fc-binding proteins, such as neonatal Fc
210 receptor (FcRn), to bind both human and bat IgG with high affinities [29]. This allowed us to
211 compare the effect of temperature on the Fc-mediated interactions of bat (*M. myotis* and *N.*
212 *noctula*) and human IgG with distinct Fc-specific proteins (Fig. 3c). Real-time binding profiles
213 and kinetic analyses of interactions with complement protein C1q (Fig. 3d), FcRn receptor
214 (Fig. 3e) and protein G (Fig. 3f) showed that temperature negatively impacts binding of all
215 studied proteins to both human and bat IgG (Fig. 3d, e, f) – an effect opposite to the one
216 observed for the Fab-dependent interactions.

217 Collectively, the results obtained indicate that the phenomenon of increasing antigen binding
218 diversity in bat IgG at elevated temperatures is specifically associated with the variable regions
219 of antibodies.

220

221 **Particular physicochemical qualities of bat antibodies can contribute to their temperature**
222 **sensitivity**

223 To get an insight into the molecular mechanism of the noncanonical diversification of immune
224 specificities in bat antibodies, we studied their molecular properties. First, we estimated the
225 thermodynamic stability of IgG molecules using a thermal shift assay. The unfolding

226 temperature (or melting point Tm) of *M. myotis* IgG was significantly lower than that of human
227 IgG (Fig. 4a), indicating lower thermodynamic stability. This was also confirmed using another
228 bat species, *Myotis capaccinii*, (Supplementary Fig. 11). It is important to note that this assay
229 measures global stability of IgG and cannot distinguish the difference in stability of different
230 domains or fragments of the molecule.

231 Additionally, we compared the overall hydrophobicity of IgG from human and *M. myotis* using
232 hydrophobic interaction chromatography. The resulting elution profiles indicated that the
233 overall hydrophobicity of bat and human IgG molecules showed negligible difference (Fig.
234 4b). This is in accordance with the relatively high sequence similarity of bat and human Fc
235 fragments (Supplementary Fig. 10). The estimation of bulk antibody hydrophobicity, however,
236 cannot provide details about the implications of different types of non-covalent forces during
237 the interaction with an antigen. To this end, we studied the effect of ionic strength on the
238 antibody-antigen binding process (Fig. 4c). The IgG from the two bat species, *M. myotis* and
239 *N. noctula*, showed specific V-shaped responses to variations in NaCl concentration upon
240 binding to distinct antigens (Fig. 4c). This pattern was different from the one observed in human
241 antibodies. Interaction of bat antibodies with antigens was favored in an environment with both
242 low and high ionic strength. This implies antigen binding involving both polar and hydrophobic
243 components (Fig. 4c). Notably, these data also suggest that at physiological concentration of
244 NaCl (0.15 M), the contribution of polar interactions is highly reduced and binding to antigens
245 is primarily driven by hydrophobic forces (Fig. 4c).

246 To better understand the difference in binding behavior of bat and human antibodies, we
247 analyzed the sequences of human and bat antibody variable regions. As annotated V_H family
248 gene sequences are not yet available for *M. myotis* or any of our study species, we used those
249 from a previous work on the closely related *Myotis lucifugus* [30]. Sequence comparison of bat
250 (n=75) and human (n=56) V_H3 genes (the most frequently used in human) revealed no

difference in their overall organization. However, *in silico* analysis (computing the GRAVY index) showed that heavy chain variable regions of bat antibodies were characterized by significantly higher hydrophobicity (less negative GRAVY index value, Fig. 4d), most evident in framework region 1 and CDR H2 (Fig. 4d).

Taken together, the results underline several physicochemical differences in bat antibodies that are not typically found in their human counterparts. These specific qualities might be associated with untypical binding properties of bat antibodies as a function of temperature.

Higher prevalence of polyreactive antibodies in bat immune repertoires is associated with temperature sensitivity

Previous studies on murine monoclonal IgG and human Fab fragments have demonstrated that polyreactive antibodies (or Fab), contrary to monoreactive ones, bind to an increased number of antigens at high temperatures [31,32]. To contextualize these findings within our study, we analyzed the reactivity of ED38, a widely used human monoclonal polyreactive antibody, as well as of two monoreactive antibodies: VRC01 (specific for gp120 of HIV-1) and S309 (binding to S proteins of both SARS-CoV-1 and SARS-CoV-2). We performed an ELISA at 4, 22 and 42 °C using the same panel of antigens that we used for our bat IgG experiments (Fig. 1a). As expected, the polyreactive ED38 significantly increased its binding to most antigens as a function of temperature (Fig 5a and Supplementary Fig. 12). An opposite effect was even observed in the case of monocreactive IgG1 (VRC01), where binding to gp120 slightly decreased at 42 °C (Fig. 5a). To test whether temperature-sensitivity of bat IgGs was mediated by elevated prevalence of polyreactive antibodies, we applied a molecular probe, dinitrophenol (DNP) conjugated to BSA. This has been proven reliable for the estimation of overall levels of polyreactive antibodies in antibody repertoires [33,34]. Indeed, IgG from *M. myotis* and *N. noctula*

275 demonstrated a considerably higher reactivity (2-3-fold) to immobilized DNP at 22 °C as
276 compared to human IgG (Fig. 5b). The same probe successfully distinguished polyreactive
277 from monoreactive antibodies (Fig. 5c). Similar results were obtained with additional probe for
278 polyreactivity – the hydrophobic hapten protoporphyrin IX (Supplementary Fig. 13), as well
279 as by immunoblot and immunofluorescence analyses (Fig. 5d and 5e). There, IgG from *M.*
280 *myotis* and *N. noctula* demonstrated high reactivity to proteins present in a *M. myotis* epithelial
281 cell lysate at 22 °C (MmNep, Fig. 5d). Notably, this binding further increased at lower ionic
282 strength (Fig. 5d) – another behavior typical for polyreactive antibodies[35]. Polyreactivity and
283 autoreactivity of bat IgG were also evident by the presence of substantial binding to autologous
284 epithelial cells (Fig. 5e). Thus, this interaction was detectable even at 22 °C; albeit at
285 significantly lower extent as compared to elevated temperature (Fig. 5e and 5f, and Fig. 7), In
286 contrast, human IgG bound only negligibly to human cells at both 22 and 42 °C (Fig 1d, Fig.
287 6).

288 Overall, these data suggest that bat antibody repertoires contain considerably higher levels of
289 polyreactive antibodies. This could partly account for the diversification of their antigen-
290 binding reactivity at high temperatures.

291

292 **Elevated temperature preferentially triggers reactivity of bat antibodies to dead cells**

293 To gain insight into the physiological role of temperature-sensitive IgG, we investigated the
294 capacity of bat and human antibodies to opsonize human endothelial cells. The marked
295 intensification of bat metabolic rate during flight is associated not only with increased body
296 temperature but also with the release of ROS, which can result in cell death and liberation of
297 various endogenous molecules with pro-inflammatory activity (DAMPs) [1]. The temperature-
298 dependent augmentation of antibody reactivity to mammalian proteins may serve as a

299 mechanism for clearing damaged or dead cells, which possess potent pro-inflammatory
300 potential. To test this hypothesis, we modeled induction of cell death by oxidative stress
301 through the exposure of human endothelial cells (HMEC-1) to hydrogen peroxide. The gating
302 strategy for identification of necrotic endothelial cells is presented in Figure 6a. Labeling cells
303 with annexin V and propidium iodide clearly indicated that exposure to oxidative stress
304 triggered endothelial cell death. To assess the impact of temperature on the reactivity of *M.*
305 *myotis* and human IgG to cells with different viability, we incubated antibodies at 22 and 42 °C
306 and tested their capacity to opsonize alive and dead cells by flow cytometry (Fig. 6b). Both
307 human and bat IgG exhibited low reactivity to alive HMEC-1 cells, which remained largely
308 unchanged when incubation was performed at high temperature (Fig. 6b). Antibody reactivity
309 to dead cells at 22 °C was also low for both human and bat samples, yet bat antibodies
310 demonstrated a significant increase in binding (Fig. 6c). In contrast, at 42 °C, binding of bat
311 IgG to dead cells was significantly augmented (Fig. 6b and 6c), while reactivity of human IgG
312 was not modified by the increase in temperature.

313 To extend these studies with bat autologous cells, we evaluated the reactivity of *M. myotis* IgG
314 to live and dead epithelial cells from the same species (Fig. 7). Those experiments demonstrated
315 the capacity of bat IgG to bind to live and dead cells at 22 °C (Fig. 7b), which further confirmed
316 the high frequency of polyreactivity and autoreactivity in bat antibody repertories (Fig. 5).
317 Importantly, at elevated temperature (42 °C), bat antibodies significantly increased their
318 binding to dead but not to alive epithelial cells (Fig. 7b and 7c). These results are consistent
319 with the data obtained with endothelial cells (Fig. 6).

320 Together, these data indicate that bat antibodies acquire preferential reactivity to dead
321 endothelial and epithelial cells at elevated temperatures. This likely facilitates the efficient
322 opsonization and rapid clearance of such cells during a metabolically active physiological state,
323 thereby exerting an important anti-inflammatory effect.

Discussion

The present study draws a direct link between specific life history traits and physiological characteristics of bats and the function of their immune compartments. In particular, we demonstrated that temperature fluctuations, accompanying daily and seasonal cycles of bats, can regulate the extent of antigen binding strength and diversity in their antibody repertoires. By elucidating the reactivity of IgG antibodies from two temperate bat species, the Greater mouse-eared bat (*Myotis myotis*) and the Common noctule (*Nyctalus noctula)*, we found that elevated temperatures (40-42 °C), typical for the active metabolic state during flight, significantly broadened their spectrum of recognized antigens. On the other hand, at temperatures representing inactive metabolic states (shallow torpor, 22 °C, or hibernation, 4 °C), diversity of antigen binding specificities of bat antibodies substantially collapsed. The same temperature changes did not modulate binding diversity of human antibodies or antibodies from other mammalian and bird species. Of note, these results are derived from several independent experiments with multiple bat serum pools, collected at different times of the year (including before and after hibernation) from three different locations. This reliably proves that antibody temperature-sensitivity is a stable trait in our study species. Furthermore, the application of highly diverse protein microarrays (containing >17000 proteins) in the study indicates that the observed phenomenon is not limited to a particular type of antigens and might have a broad physiological relevance. Lastly, obtaining equivalent results from species belonging to two genera with distinct life history traits indicates that antibody temperature-sensitivity might be widely distributed among order Chiroptera.

The study also demonstrated that the sensitivity of bat antibodies to temperature fluctuations is mediated by the antigen-binding fragment of the immunoglobulin molecule but not by regions in its constant portion. Previous research demonstrated that interactions of murine polyreactive

349 antibodies, or human polyreactive Fab fragments, were exclusively augmented at high
350 temperatures in contrast to those of monoreactive antibodies (or Fab fragments) [31,32], an effect
351 that we confirmed here with human monoclonal IgGs. Indeed, our data from different
352 orthogonal approaches indicates that bat IgG repertoires have a higher prevalence of
353 polyreactive antibodies as compared to human repertoires. This likely contributes to
354 temperature-sensitivity and antibody repertoire diversification in these species. Yet, we do not
355 exclude the implication of other (not mutually exclusive) mechanisms, especially in the cases
356 of antigens recognized with high binding affinities (NS1 of TBEV and rabies virus
357 glycoprotein). Indeed, our biochemical analyses revealed some unusual physicochemical
358 features of bat IgG, such as significantly lower thermodynamic stability and distinctive
359 implication of both polar and hydrophobic forces in the antigen binding process. The
360 thermodynamic stability of proteins is determined by the complexity of noncovalent interaction
361 networks maintaining the protein fold. Thus, polypeptide chains of less stable proteins are
362 usually less tightly packed and characterized by increased structural dynamics [36,37], which can
363 be further enhanced as a function of temperature. This is probably the case of bat antibodies
364 where higher flexibility of the antigen-binding site probably allows increased binding
365 adaptability, recognition of a large number of antigens [38-40], or targeting epitopes difficult to
366 recognize by conventional antibodies [41]. Another physiochemical quality of bat IgG is their
367 unique reliance on polar and hydrophobic forces for antigen binding upon variation of ionic
368 strength. Thus, despite the presence of polar groups in antigen binding sites, at physiologically
369 relevant ionic strength, bat antibody-antigen interaction seems to be mainly driven by
370 hydrophobic forces. This agrees with the sequence analyses of immunoglobulin genes showing
371 that some regions in heavy chain variable domains (framework region 1 and CDRH2) in bats
372 have significantly higher hydrophobicity as compared to their human counterparts. Together,
373 these findings may explain the temperature effects as it was found that molecular interactions

374 that are mainly driven by hydrophobic forces increase their strength as function of temperature
375 [42,43] – a fact in full concordance with our data.

376 The unconventional mechanism for control of antigen binding diversity, proposed here, could
377 further explain disease tolerance in bats and may also have other important biological
378 repercussions. Immunogenetic studies have demonstrated that the diversity of functional gene
379 segments encoding variable immunoglobulin regions in bats is similar to that of humans and
380 mice [30,44-46]. Thus, the potential repertoire of bat antibody specificities seems sufficiently large
381 to cope with high versatility of pathogens, without the need for any extraordinary
382 diversification strategies. Yet, immune reactivity of bat antibodies that correlates to (and is
383 controlled by) the state of metabolic activity might be biologically meaningful by providing a
384 physiological adaptation for optimizing immune response timing. For instance, reducing
385 antibody reactivity at low temperatures might be an additional strategy to economize energy
386 and resources during phases of inactivity and suppressed metabolism, i.e., daily torpor or
387 seasonal hibernation [47,48]. As pathogen replication is severely inhibited at low temperatures
388 typical for torpor, some immune components may not be necessary to control infection during
389 this period. This is particularly true for adaptive immune responses that are known to be one
390 of the most energy-demanding processes in mammals [49,50]. On the other hand, substantial
391 antibody diversification observed at high temperatures may provide bats with instant protection
392 upon exiting torpor and returning to body temperatures that are favorable for pathogen
393 replication. Such acting at the first line of immune defense is typical for polyreactive antibodies
394 that allow the immune system to rapidly cover a practically infinite antigenic space, albeit with
395 lower affinity. Interestingly, however, bat IgG also shows a temperature-dependent rise in
396 binding strength to specific antigens as exemplified by our ELISA and real-time kinetic
397 experiments with NS1 protein of TBEV and rabies virus glycoprotein. Both have been
398 previously detected in the bat species used in our study [51-54]. Therefore, the apparent binding

399 affinity of bat IgG to them at high temperature may indicate immune repertoire shaping as a
400 result of coevolution with these or other related viruses.

401 Another important aspect of bat antibody temperature-sensitivity is the potential to control
402 inflammation induced by the accumulation of dead cells and the release of DAMPs during
403 active metabolic states. This is in full concordance with previous research suggesting the
404 evolution of powered flight as a main driver of immune system evolution in bats [9,55,56]. Indeed,
405 flight in bats is associated with a substantial increase in metabolic rate (>30 folds), rise in body
406 temperature, and intensification of oxidative processes that can lead to cell damage and the
407 release of various DAMP molecules such as DNA, misfolded proteins, oxidized phospholipids,
408 ATP, etc [1,22,57,58]. As an adaptation to such metabolic stress, the activity of innate pathways
409 sensing these molecules is reduced in bats, thus protecting them from perpetual inflammation
410 [8,9,55] – a phenomenon that has also been associated with bat tolerance to viral infections [9,59].
411 Our study provides yet another anti-inflammatory mechanism in bats by showing that bat IgG
412 preferentially binds and opsonizes dead human endothelial or bat epithelial cells while sparing
413 living cells at elevated temperatures. Thus, the increase in antibody reactivity during active
414 metabolic states probably contributes to the clearance of apoptotic cells and damaged
415 macromolecules *in vivo*. The distinction between healthy and damaged cells by bat antibodies
416 can be based on one or several hallmarks typical for dying eukaryotic cells – changes in
417 membrane phospholipids composition, membrane permeabilization, appearance of cryptic and
418 oxidized epitopes, etc [60, 61, 62]. Studies in mouse models and humans have confirmed the
419 important role of natural polyreactive antibodies in the maintenance of immune homeostasis
420 through the clearance of damaged or dead cells [60,63-65]. This is in accordance with our data
421 showing that a considerable fraction of bat antibodies are polyreactive.

422 Taken together, the findings from this study uncover new features of bat immune system and
423 provide additional explanation of bat tolerance to inflammation and disease. We also depict an

alternative mechanism for diversification of immune specificity of antibodies in general and highlight the link between metabolism and immunity. Further elucidating the mechanism of temperature sensitivity of bat antibodies will extend our understanding about evolution of immune system in mammals and can lead to practical discoveries with important repercussions for human health.

Methods

Bat capture and blood sampling

For this study, we used samples from 4 bat species from two genera: Greater moused-eared bat (*Myotis myotis*), Lesser mouse-eared bat (*Myotis blythii*), Long-fingered bat (*Myotis capaccinii*), and Common noctule (*Nyctalus noctula*). Greater moused-eared bats were caught at Ivanova voda cave, situated in Western Rhodopes mountain, Bulgaria (N41.894, E24.880), in April 2021 (n = 40), October 2021 (n = 45), May 2022 (n = 29) and October 2023 (n=20) as well as in Orlova chuka cave, situated in Northern Bulgaria (N 43.5932, E 25.9601), in September 2023 (n=50). Lesser mouse-eared bats were caught in Ivanova voda in October 2023 (n=18) and in Orlova Chuka cave in September 2023 (n=10). Long-fingered bats were also caught at Ivanova voda in April 2021 (n = 3), May 2022 (n = 20), and October 2023 (n=12). Noctule bats were caught at Devetashkata cave, situated in North Central Bulgaria (N43.233, E24.885), in June 2022 (n=18) and August 2023 (n=71). All bats were caught at cave entrances at sunset using a harptrap (for Ivanova voda and Orlova chuka) or mistnets (for Devetashkata cave), then they were kept in individual cotton bags until processing. Their sex, size, weight, and age group (adult/juvenile) were noted. For species identification, we followed Dietz and Von Helversen (2004). The research was carried out under permits by the Bulgarian Biodiversity Act (No 830/19.09.2020 and No 927/04.04.2022).

448 Blood samples were taken from the uropatagium vein by puncturing it with a sterile disposable
449 insulin needle and collecting the few drops of leaked blood (most often below 100 µL) using a
450 sterile disposable hematocrit capillary or a pipette with sterile disposable tips. Blood sampling
451 of this kind is not supposed to affect survival rates of bats [66]. Blood serum was immediately
452 separated from plasma by centrifugation for 15 to 30 mins at 2000 rpm. Separated sera were
453 then frozen at -20 °C. Each sampled bat was given water and mealworms (*Tenebrio*) to
454 compensate for blood loss when appropriate. We minimized handling time to reduce stress on
455 the animals. All researchers used personal protective equipment (masks, gloves) and non-
456 disposable instruments and working surfaces were disinfected between each animal. To obtain
457 enough material for the experiments, usually we pooled sera from 3 to 10 individuals directly
458 in the field or in the lab.

459

460 *Samples from human and other species*

461 In the study we used fresh AB serum samples from ten anonymised healthy human donors,
462 obtained under the ethical convention between INSERM with Etablissement Français du Sang
463 #18/EFS/033. Pooled sera from different mammals: mouse (*Mus musculus*), rabbit
464 (*Oryctolagus cuniculus*), goat (*Capra hircus*), and cattle (*Bos taurus*) were obtained from
465 Sigma-Aldrich (St. Louis, MO, USA).

466 The sera from four bird species: snowy owl (*Bubo scandiacus*, n=2), Egyptian vulture
467 (*Neophron percnopterus*, n=2), Eurasian griffon vulture (*Gyps fulvus*, n=2), and Carrion crow
468 (*Corvus corone*, n=4), are part of the Zoo de la Palmyre (Les Mathes, Charente-Maritime,
469 France) serobank used as part of a study designed to estimate the circulation of WNV and
470 USUV flaviviruses in captive avifauna. This study was approved by the Ethics Committee for

471 clinical Research (ComERC) of Veterinary school of Alfort (EnVA) (Agreement number: 2023-
472 06-23).

473 *IgG purification*

474 Total IgG from human, bat (*M. myotis*, *M. blythii*, *M. capaccinii* and *N. noctula*), and other
475 mammalian sera was purified using Melon^{TM} Gel IgG Spin Purification Kit (Thermo Fischer
476 Scientific, Waltham, MA) according to the manufacturer's protocol, with the sole exception
477 that centrifugation was performed for 30 sec instead of 10 sec. Concentration of purified IgG
478 was measured by a Nanodrop spectrophotometer (Thermo Fischer Scientific) and its purity was
479 confirmed by SDS-PAGE performed in reducing and non-reducing conditions.

480 Alternatively, IgG from *M. myotis* and *N. noctula* was purified using protein G agarose
481 (Thermo Fisher Scientific).

482

483 *Purification of bat albumin*

484 Albumin from *M. myotis* was purified from the eluate of Melon^{TM} Gel matrix obtained after
485 exposure of the matrix to PBS after purification of IgG. Samples were diluted in a large volume
486 (5.5 × excess) of binding buffer (50 mM KH_2PO_4, pH 7.0) and applied on a 1 mL HiTrap Blue
487 HP column (Cytiva, Life Sciences, Wilmington, DE) previously equilibrated with binding
488 buffer. The column was washed with 30 mL binding buffer and elution was obtained with a
489 linear gradient of 1.5 M potassium chloride. Albumin purity was confirmed by SDS-PAGE.
490 The bat albumin was biotinylated using EZ-Link® NHS-SS-Biotin (Thermo Fisher Scientific,
491 Ref#21441) following a protocol recommended by the manufacturer. In brief, albumin (19.6
492 μM) was exposed to 10 × excess of EZ-Link® NHS-SS-Biotin (10 mM stock in DMSO) for 1
493 hour at room temperature. The reaction was stopped by adding 1M Tris pH 8 to a final
494 concentration of 20 mM.

495

496 *Generation of bat F(ab')$_2$ fragments*

497 Purified IgG from *M. myotis* was digested by recombinant IdeS protease from *Streptococcus*
498 *pyogenes* (kindly provided by Dr. Sébastien Lacroix-Desmazes, Centre de Recherche des
499 Cordeliers, Paris France). The reaction was performed in PBS at a 1:25 (enzyme:substrate)
500 ratio for 16 hours at 25 °C. After, the reaction mixture was additionally incubated with protein
501 G agarose (Thermo Fisher Scientific) to remove undigested IgG and Fc fragments. For every
502 100 µl of sample, 25 µl of protein G-agarose gel slurry was applied.

503

504 *ELISA assays*

505 - *Temperature dependence of antigen binding of bat and human IgG*

506 Thermo Scientific™ Nunc 384-Well Clear Polystyrene Plates (Thermo Fischer Scientific) were
507 coated overnight at 4 °C (or alternatively for 2 hours at room temperature, 22-24 °C) with the
508 following molecules: human Factor VIII (Helixate® FS, CSL Behring, King of Prussia, PA);
509 human Factor IX; human von Willebrand factor (both from LFB, Les Ulis, France); human
510 insulin, human hemopexin, human hemoglobin, porcine thyroglobulin, bovine histone III,
511 equine cytochrome C, lipopolysaccharide from *Escherichia coli* O55:B5 (all from Sigma-
512 Aldrich); LysM protein (from *Enterococcus faecalis*, kindly provided by Dr. Stephane
513 Mesnage, University of Sheffield, UK); Asp f1 protein (from *Aspergillus fumigatus*, kindly
514 provided by Dr. Vishu Kumar Aimanianda, Institute Pasteur, Paris); spike protein of SARS-
515 CoV-2 (S protein, Wuhan variant), receptor-binding domain (RBD, SARS-CoV-2 Wuhan
516 variant), human ACE2 (the three proteins were kindly provided by Dr. Hugo Mouquet, Institute
517 Pasteur, Paris, France); gp120 from HIV-1 (strain CN54, kindly provided by NIH AIDS
518 Reagents Program); rabies virus glycoprotein, Ebola Zaire virus glycoprotein, Nipah virus

519 glycoprotein, Hendra virus glycoprotein, NS1 protein of tick-born encephalitis virus (TBEV),
520 measles virus mosaic hemagglutinin, HA(ΔTM)(A/California/04/2009)(H1N1), hepatitis D
521 virus small Ag (HDVAg), Dengue virus 2 Capsid Protein, Chikungunya virus Capsid protein,
522 HPV-16 L2 protein, Antigen Mpt70 (*M. tuberculosis*/H37Rv), Antigen 85-B (*M.*
523 *tuberculosis*/H37Rv), and p47 (*T. pallidum*/Nichols strain). All viral and bacterial proteins
524 listed afterwards gp120 were obtained from Immune Technology Corp. (New York, NY, USA).
525 Plates were incubated with proteins usually diluted to 5 μg/ml in PBS; insulin and LPS were
526 diluted at 10 μg/ml. After the coating step, plates were blocked by incubation for 2 hours with
527 PBS containing 0.25 % Tween 20. Alternatively, other blocking agents were applied: 1 %
528 solution of bovine serum albumin (Sigma-Aldrich) in PBS or 1 × solution of synthetic block
529 (Thermo Fisher Scientific) in PBS. Plates were then incubated with: IgG purified from pooled
530 sera of two bat species, *M. myotis* and *N. noctula*; IgG purified from pooled sera of healthy
531 humans; IgG purified from pooled sera of other mammals: mouse (*M. musculus*), rabbit (*O.*
532 *cuniculus*), goat (*C. hircus*), and cattle (*B. taurus*); and human monoclonal IgG1 antibodies
533 ED38 (highly polyreactive), VRC01 (specific for HIV-1 gp120), and S309 (specific for RBD
534 of SARS-CoV-2), serving as controls. Polyclonal IgG from human, bats, and other mammals
535 was typically diluted to 0.07 mg/ml (or wherever indicated to 0.02 or 0.1 mg/ml) in PBS
536 containing 0.05 % Tween 20 (T-PBS). Monoclonal IgG antibodies were diluted to
537 concentrations of 0.01 and 0.07 mg/ml in T-PBS. In a specific experimental setting, reactivity
538 of IgG in whole sera from *M. myotis* or human were tested. To this end, sera were diluted 200
539 × in T-PBS. In another experiment, plates were incubated with sera from different species of
540 birds: snowy owl (*B. scandiacus)*, Egyptian vulture (*N. percnopterus)*, Eurasian griffon vulture
541 (*G. fulvus)*, and Carrion crow (*C. corone)*, diluted 100 × in T-PBS. The purified polyclonal IgG
542 from bats, humans, other mammals or monoclonal human IgG1 antibodies as well as diluted
543 sera from human, bats and birds, were incubated for 2 hours with immobilized antigens in

544 parallel at three different temperatures: 4 °C, 22 °C, and 42 °C (one plate per temperature).
545 After, the microtiter plates were washed 5 × with T-PBS and then incubated for 1 hour at room
546 temperature with 2 μg/ml of biotinylated recombinant protein G (Pierce™, Thermo Fisher
547 Scientific) for recognition of IgG antibodies from human, bats, and other mammalian species.
548 Following thorough washing, streptavidin conjugated with HRP (Invitrogen, Thermo Fisher
549 Scientific) diluted 100 × was added and incubated for 30 min at room temperature. For
550 detection of bird's IgY antibodies, plates were incubated with goat anti-chicken IgY-HRP
551 (Southern Biotech, AL, USA), diluted 3000 × in T-PBS. This antibody showed high cross-
552 reactivity for IgY from different bird species. After thorough washing with T-PBS, reactivity
553 of antibodies was revealed by adding peroxidase substrate, *o*-phenylenediamine
554 dihydrochloride (Sigma-Adrich). After stopping the reaction with 2M HCl, the absorbance was
555 measured with a microplate reader (Infinite 200 Pro, Tecan, Männedorf, Switzerland) at 492
556 nm.

557 - *Titration of bat and human sera*

558 NS1 protein of tick-born encephalitis virus (TBEV), rabies virus glycoprotein, influenza
559 hemagglutinin, and SARS-CoV-2 S protein were immobilized at 2 μg/ml on 96-well
560 polystyrene microtiter plates Nunc MaxiSorp™ (Thermo Fisher Scientific). Following
561 blocking with 1 × synthetic block (Thermo Fisher Scientific) in PBS, whole sera from human
562 and *M. myotis* was serially diluted (starting from 60 × to 1920 ×) in T-PBS and incubated for 2
563 hours at 4 °C, 22 °C, 42 °C with immobilized antigens (human serum with SARS-CoV-2 S
564 protein and influenza A hemagglutinin; bat serum with TBEV NS1 and rabies virus
565 glycoprotein). Detection of bound bat IgGs was done by incubation for 1 hour at room
566 temperature with mouse anti-bat immunoglobulin (L-chain specific, clone BT1-4F10, Novus
567 Biologicals, CO, USA) diluted to 1 μg/ml in T-PBS followed by incubation for 1 hour with

568 goat-anti mouse IgG conjugated with HRP (Southern Biotech) diluted 2000 × in T-PBS.
569 Binding of human IgG was detected by 1 hour incubation at room temperature with anti-human
570 IgG, conjugated with HRP (clone JDC-10, Southern Biotech) diluted 3000 × in T-PBS.
571 Succeeding steps of the experiment were identical to those described for the previous ELISA
572 setting.

573 - *Comparison of the reactivity of bat albumin and bat IgG with crude extract of bat*
574 *epithelial cells*

575 Total lysate of the nasal epithelial cell line (MmNep) [67] of *M. myotis* was prepared by freezing
576 thoroughly washed with PBS cells (6.3×10^7 cells in 1 ml PBS). After thawing, the suspension
577 was immediately sonicated and centrifugated at 10000 rpm for 10 min. The total protein
578 concentration of the supernatant was determined by Nanodrop. The crude extract was coated
579 on Nunc 384-Well Clear Polystyrene Plates (Thermo Fischer Scientific) at a concentration of
580 20 µg/ml in PBS for 2 hours at room temperature. Plates were blocked by a solution of 0.25 %
581 of Tween 20 in PBS. Purified IgG and biotinylated albumin from *M. myotis,* were incubated at
582 serial dilutions ranging 200 – 3.125 nM in T-PBS for 1 hour. Identical samples were incubated
583 at 4 °C, 22 °C, and 42 °C. After washing, plates were incubated for 1 hour with 2 µg/ml
584 biotinylated protein G in T-PBS for detection of bat IgG. The IgG and albumin reactivity to
585 cell antigens was detected by incubation for 1 hour with streptavidin-HRP (Thermo Fischer
586 Scientific) diluted 100 × in T-PBS. Succeeding experimental steps were identical to the
587 principal ELISA experiment described above.

588 - *Temperature sensitivity of antigen binding of $F(ab')_2$ fragments from bat IgG*

589 Thermo Scientific™ Nunc 384-Well Clear Polystyrene Plates (Thermo Fischer Scientific) were
590 coated for 2 hours at room temperature with 5 µg/ml of rabies virus glycoprotein, NS1 protein
591 of tick-born encephalitis virus (TBEV), measles virus mosaic hemagglutinin, Antigen Mpt70

592 (*M.Tuberculosis*/H37Rv), and p47 (*T. pallidum*/Nichols strain) in PBS. Plates were blocked
593 with PBS containing 0.25 % Tween 20 for 1 hour at room temperature followed by incubation
594 for 1 hour with 10 μg/ml of $F(ab')_2$ fragments from *M. myotis* in parallel at 4 °C, 22 °C and 42
595 °C. Detection of bound bat $F(ab')_2$ fragments was done by incubation for 1 hour at room
596 temperature with mouse anti-bat immunoglobulin (L-chain specific, clone BT1-4F10, Novus
597 Biologicals, CO, USA) diluted to 1 μg/ml in T-PBS followed by incubation for 1 hour with
598 goat-anti mouse IgG conjugated with HRP (Southern Biotech) diluted 2000 × in T-PBS.

599 - *Ionic strength dependence of binding of human and bat IgG*

600 Half-area 96-well polystyrene plates (Greiner-Bio-One, Les Ulis, France) were coated by
601 incubation for 2 hours at room temperature with 2 μg/ml of NS1 protein of tick-born
602 encephalitis virus (TBEV), rabies virus glycoprotein, influenza hemagglutinin, measles virus
603 mosaic hemagglutinin, SARS-CoV-2 S protein, and LysM from *E. faecalis* in PBS. After, plates
604 were blocked by 1 hour incubation with a solution of PBS containing 1 × synthetic block
605 (Thermo Fisher Scientific) and 0.25 % Tween 20. Purified human and bat (*M. myotis* and *N.*
606 *noctula*) IgG was diluted to 20 μg/ml in 10 mM HEPES pH 7.5, 0.05 % Tween 20 buffer
607 containing increasing concentrations NaCl: 0, 0.0078 – 4 M, then it was incubated for 2 hours
608 at 42 °C. Bat antibodies were incubated with: TBEV NS1, measles virus hemagglutinin, and
609 rabies virus glycoproteins; human antibodies were incubated with: influenza hemagglutinin,
610 SARS-CoV-2 S protein, and LysM from *E. faecalis.* Following steps were as in the principal
611 ELISA experiment described above.

612 - *Interaction of bat and human IgG with protoporphyrin IX*

613 Protoporphyrin IX (Sigma-Alrich) was covalently conjugated on the surface of gelatin pre-
614 coated half-area 96-well polystyrene plates (Greiner-Bio-One) following an amino-coupling
615 procedure previously described for heme [68]. The hapten-coated plates were blocked for 1 hour

616 with 0.25 % solution of Tween 20 in PBS. Purified pooled IgG from bat (*M. myotis*) and human
617 were serially diluted in the range 100 – 1.562 μg/ml (670 – 10.468 nM) in T-PBS and incubated
618 for 90 min at room temperature. Next steps for the detection of bound IgG were as in the
619 principal ELISA experiment described above.

620 – *Assessment of polyreactivity of IgG antibodies*

621 To assess the level of polyreactive antibodies in polyclonal bat and human IgG samples, we
622 used an established assay based on the analyses of antibody reactivity to a nitroarene hapten [34].
623 Ninety-six well polystyrene plates NUNC MaxiSorp™ or NUNC 384-Well Clear polystyrene
624 plates (Thermo Fisher Scientific) were coated with 2,4-dinitrophenyl conjugated to BSA (DNP-
625 BSA, Sigma-Aldrich), diluted to 10 μg/ml in PBS and incubated for 2 hours at room
626 temperature (22-24 °C). As a control, unconjugated BSA was coated under identical conditions.
627 Plates were blocked by saturation with a 0.25 % solution of Tween 20 in PBS for 1 hour at
628 room temperature. For evaluation of antibody reactivity to DNP, IgG purified from human and
629 bat (*M. myotis* and *N. noctula*) pooled sera was diluted to 670 nM (100 μg/ml) in PBS-T,
630 followed by two-fold serial dilution to 10.468 nM (1.56 μg/ml). Monoreactive (VRC01 and
631 S309) and polyreactive (ED38) monoclonal IgG1 antibodies were used as controls. These were
632 first diluted to 400 nM (60 μg/ml) followed by three-fold serial dilutions to 0.0068 nM (0.001
633 μg/ml) in PBS-T. Polyclonal and monoclonal antibodies were incubated on microtiter plates
634 for 1 hour at room temperature. Following steps were as described above.

635

636 *Real-time interaction analyses – temperature dependence of antigen binding of bat IgG*

637 Interaction of bat IgG with selected viral proteins was evaluated by a surface plasmon
638 resonance-based system – Biacore 2000 (Cytiva, Biacore, Uppsala, Sweden). Recombinant
639 rabies virus glycoprotein and NS1 protein of TBEV were covalently immobilized on CM5

640 sensor chips (Cytiva, Biacore) using an amine-coupling kit (Cytiva, Biacore) according to the
641 procedure recommended by the manufacturer. In brief, viral proteins were diluted to a final
642 concentration of 10 µg/ml in 5 mM maleic acid, pH 4, and injected over pre-activated sensor
643 surfaces. Carboxyl groups of the carboxymethylated dextran were activated by exposure of the
644 surface for 4 min to a mixture of 1-ethyl-3-(3-dimethylaminopropyl)-carbodiimide and N-
645 hydroxysuccinimide. For inactivation of the activated carboxyl groups that were not engaged
646 in interactions with the amino groups from the proteins, sensor surfaces were exposed for 4
647 min to 1M solution of enthanolamine.HCl. Covalent immobilization of viral proteins and all
648 kinetic measurements were performed with HBS-EP (10 mM HEPES pH 7.2; 150 mM NaCl;
649 3 mM EDTA, and 0.005 % Tween 20) used as running and sample dilution buffer. Prior to real-
650 time binding analyses, the running buffer was always filtered through a 0.22 µm filter and
651 degassed under a vacuum.

652 To measure interactions of bat antibodies with viral proteins as a function of temperature, IgG
653 purified from a serum pool from *M. myotis* was serially diluted in the running buffer in the
654 range 100 – 6.25 µg/ml (670 – 41.875 nM) and injected over the sensor surface. The flow rate
655 during all interaction analyses was set at 30 µl/min. The association and dissociation phases of
656 bat polyclonal IgG binding were monitored for 4 and 5 min, respectively. Between consecutive
657 sample injections, the sensor chip surface was regenerated by a brief exposure (30 sec) to a
658 solution of 2M NaSCN (Sigma-Aldrich). All analyses were performed at the following
659 temperatures: 4, 6, 16, 24, 32, and 40 °C. Real-time binding curves were obtained after
660 subtracting bat IgG binding to a reference surface that lacked immobilized viral proteins.
661 Binding curves obtained at 40 °C allowed reliable evaluation of binding kinetics. To this end,
662 we used BIAevaluation software v. 4.1.1 (Cytiva, Biacore) performing global kinetics analyses
663 applying the Langmuir binding model. The apparent binding kinetics and affinity were

evaluated under the assumption that 10 % of all antibodies in the pooled preparation were able to bind viral proteins.

Real-time interaction analyses – temperature dependence of Fc-dependent interactions of bat and human IgG

Purified bat (*M. myotis,* n=10; and *N. noctula,* n=35)*,* and human pooled IgG were immobilized on CM5 sensor chips (Cytiva, Life Sciences, Biacore). To this end, IgG samples were diluted to a final concentration of 10 µg/ml in 5 mM maleic acid, pH 4, and injected over pre-activated sensor surfaces. Other parameters of the immobilization procedure were identical as described above.

To assess the temperature-dependence of Fc-mediated interactions of IgG, the binding of human C1q (Comptech, TX, USA), recombinant human FcRn (kindly provided by Dr. Sune Justesen, Immunitrack Aps, Copenhagen, Denmark), and recombinant protein G (Pierce™, Thermo Fisher Scientific) was elucidated. The real-time interaction analyses with C1q and protein G were performed in HBS-EP buffer. The analyses of the binding of FcRn to IgG were studied in a buffer containing 100 mM NaCl, 100 mM Tris pH 5.7 (adjusted with dry citric acid), and 0.1 % Tween-20. C1q was injected after dilution to 0.625 nM; FcRn was injected at serial dilutions in the range: 25 - 0.097 nM (2 × dilution step); the binding of protein G was measured at serial dilutions in the range: 100 – 0.046 nM (3 × dilution step). Buffer flow rate during all interaction analyses was set at 30 µl/min. The association and dissociation phases of all interactions were monitored for 4 and 5 min, respectively. Between the injections of Fc-binding proteins, the sensor chip surface was regenerated by a brief exposure (30 sec) to a solution of 1.5M NaSCN (in the case of C1q); 100 mM NaCl, 100 mM Tris with pH 7.8 (in the case of FcRn), and a solution of 2M NaOH and 0.1 M NaOH (in the case of protein G). The real-time binding measurements were performed as a function of temperature at 4, 22 and 40

689 °C (for C1q) and at 22 and 40 °C (for FcRn and protein G). For data analyses BIAevaluation
690 software v. 4.1.1 (Cytiva, Biacore) was used for performing global kinetics analyses applying
691 the Langmuir binding model.

692

693 *Immunoblot analyses*

694 Cell lysate of MmNep cells (epithelial cells, *Myotis myotis*) [67] or *Bacillus anthracis* were loaded
695 to 1-well 4-12% Bis-Tris NuPAGE Novex SDS-PAGE gels (Invitrogen, Thermo Fisher
696 Scientific). Proteins were separated for 45 min at 200 V. After migration, they were transferred
697 to nitrocellulose membranes using an iBlot electrotransfer system (Invitrogen, Thermo Fisher
698 Scientific). Membranes were blocked overnight with PBS containing 0.1% Tween 20 (T-PBS).
699 Next, they were conditioned in PBS 1/3 × + 0.1% Tween 20 for 10 min and fixed on a Miniblot
700 system (Immunetics, Cambridge, MA). They were then incubated for 1 hour at 22 °C with IgG
701 from *M. myotis (*n=10 individuals*)* and *N. noctula* (n=35 individuals) in two-fold dilutions,
702 from 20 µg/ml to 2.5 µg/ml, in phosphate buffer (PBS) with NaCl concentration of eighter 150
703 mM or 50 mM.

704 Membranes were washed (6 × 10 min) with T-PBS and then incubated for 1 hour at room
705 temperature with 2 µg/mL biotinylated Protein-G (Thermo Fisher Scientific) in T-PBS. Next,
706 they were washed (6 × 5 min) with T-PBS 0.1% and incubated with streptavidine coupled with
707 alkaline phosphatase (Southern Biotech) diluted 2000 ×. Finally, membranes were washed (6
708 × 5 min) with T-PBS 0.1%, rinsed with water to remove phosphate ions, and revealed by
709 incubation with SigmaFast BCIP/NBT substrate solution (Sigma-Aldrich). They were then left
710 to dry for 24 hours and images were taken on the iBright CL1500 Imaging System (Thermo
711 Fisher Scientific).

712

713 *Conjugation of human and bat IgG with fluorochromes*

714 Human and bat antibodies were covalently labelled with fluorochromes via amine-coupling
715 reaction. First, polyclonal IgG purified from pooled human and bat (*M. myotis*) sera were
716 diluted to 2 μM in a solution consisting of 1/3 100 mM carbonate buffer, pH 9, and 2/3 PBS.
717 Amine-reactive Alexa Fluor™ 555 NHS ester (Thermo Fisher Scientific) was added to IgG
718 samples to a final concentration of fluorochrome 40 μM and incubated for 1 hour at room
719 temperature with constant gentle agitation. Additionally, human and bat IgG was labelled with
720 Alexa Fluor™ 647 NHS ester under identical conditions. Following the conjugation reaction,
721 we separated labelled IgG from unconjugated fluorochromes by applying PD-10 columns with
722 Sephadex G-25 resin (Cytiva, Marlborough, MA). Conjugation efficacy and conjugated IgG
723 concentration were measured by absorbance spectroscopy using Agilent Cary 100 UV-vis
724 spectrophotometer (Agilent Technologies, Santa Clara, CA).

725

726 *Immunofluorescence analyses*

727 To evaluate reactivity of bat (*M. myotis, M. blythii, M. cappaccinii, and N. noctula*) and human
728 IgG to HEp2 cells, we used the AESKUSLIDES® ANA-HEp-2 diagnostic kit for detection of
729 autoantibodies recognizing cellular antigens by immunofluorescence (Aesku Diagnostics,
730 Wendelsheim, Germany). We followed the protocol recommended by the manufacturer with
731 certain modifications. Thus, human and bat IgG conjugated to Alexa Fluor™ 555 was diluted
732 to 50 μg/ml in PBS and incubated for 30 min in a moist chamber with Hep-2 cells pre-fixed on
733 glass slides. To evaluate the reactivity of bat (*M. myotis*) IgG to bat nasal epithelial cells, we
734 cultivated MmNep [67] cells in complete DMEM/F-12+GlutaMAX™ (Gibco™, Thermo Fisher
735 Scientific) containing 10 % fetal calf serum (ATCC) and 1% Penicillin-Streptomycin (Gibco™,
736 Thermo Fisher Scientific) on coverslips (10 mm diameter). After reaching 80 % confluence,

737 the cells were fixed with 4% PFA mixed with Hoechst dye (Thermo Fisher Scientific) diluted
738 5000 ×. The coverslips were thoroughly washed after each following step. The cells were
739 permeabilized with a 0.2% Triton-X-100 solution (Sigma-Aldrich). Next, they were incubated
740 for 30 min with bat IgG coupled with Alexa Fluor™ at 25 µg/ml. Finally, the cells were
741 incubated with Phalloidin-iFluor 488 diluted 1000 × (Abcam, Cambridge, United Kingdom)
742 for 20 min. The Hoechst and Phalloidin staining were used to facilitate cell counting.

743 To evaluate the effect of temperature on IgG binding, slides with identical samples were
744 incubated at 22 °C and 42 °C. As a negative control, some cells were incubated with PBS only
745 or with 50 µg/ml of Alexa Fluor™ 555-streptavidin (Invitrogen, Thermo Fisher Scientific).
746 After washing with PBS and applying mounting medium and cover slips, immunofluorescence
747 was read by Zeiss Axio Observer Z1 microscope (Carl Zeiss AG, Oberkochen, Germany)
748 equipped with ApoTome system. The acquisition time was 80 ms (HEp-2 cells) or 50 ms
749 (MmNep cells). Acquired fluorescence images with magnifications of 63 × were coloured
750 digitally in green. The acquisition and data analyses were performed with ZEN software (Carl
751 Zeiss AG). Quantification of mean fluorescence intensity (MFI), reflecting antibody interaction
752 with the cells, was normalized by the number of cells observed in the bright field.

753

754 *Protein microarrays*

755 To evaluate the effect of temperature on the immunoreactivity of human and bat (*M. myotis*
756 *and N. noctula*) polyclonal IgG to a broad repertoire of human proteins (>17 000), we applied
757 HuProt™ v4.0 protein microarrays (CDI Laboratories, Inc., Baltimore, MD). First, microarray
758 slides were blocked by incubation for 2 hours at room temperature with PBS containing 1×
759 synthetic block (Thermo Fisher Scientific) and 0.05 % Tween 20. After washing for 5 min with
760 PBS containing 0.05 % Tween 20 (PBS-T), chips were incubated for 2 hours at 22 °C or 42 °C

761 with Alexa Fluor™ 647-conjugated human and *M. myotis* IgG (for 22 °C) and Alexa Fluor™
762 555-conjugated human and *M. myotis* IgG (for 42 °C) with constant agitation on an orbital
763 shaker (at 50 rpm). Alexa Fluor™ 555-conjugated IgG from *N. noctula* was used for analyses
764 at both 22 and 42 °C. IgG concentration was 5 μg/ml in 5 mL PBS-T. Following incubation
765 with antibodies, microarray slides were washed 3 × 5 min with PBS-T with constant agitation
766 (50 rpm). After, salts were removed by soaking the slides in 1/10 solution of PBS in deionized
767 water and dried by centrifugation (100 × g) for 1 min. Fluorescence intensity at 532 nm and
768 635 nm was measured by the microarray scanner GenePix 4000B (Molecular Devices, San
769 Jose, CA). Raw data from microarray chips were quantified and analyzed using Spotxel
770 software v. 1.7.7 (Sicasys, Heidelberg, Germany).
771
772 *Thermal shift assay for estimation of thermodynamic stability of IgG*
773 To assess the thermodynamic stability of human and bat (*M. myotis* and *M. capaccinii*) purified
774 IgG molecules, we used Protein Thermal Shift Dye Kit (Applied Biosystems, Thermo Fisher
775 Scientific) following the manufacturer's protocol. All IgG samples were diluted in PBS and
776 tested at a concentration of 80 μg/ml. Protein unfolding reactions and fluorescent signal
777 detection were performed in Applied Biosystems 7900 HT Fast Real-Time PCR machine
778 (Applied Biosystems, Thermo Fisher Scientific). For data analyses, we used GraphPad Prism
779 v. 9.5 software (GraphPad Software, San Diego, CA). Melting points (T_m) of IgG molecules
780 were calculated by fitting experimental data using the Boltzmann equation.
781
782 *Hydrophobic interaction chromatography*
783 Overall hydrophobicity of human and bat (*M. myotis*) IgG was assessed by hydrophobic
784 interaction chromatography. To this end, 70 μg of purified IgG were diluted in 1.1 M solution

785 of ammonium sulfate and injected into a 1 mL HiTrap Octyl FF column (Cytiva, Life Sciences).
786 The column was previously equilibrated with binding buffer (50 mM sodium phosphate, 1.1 M
787 ammonium sulfate, pH 7.0). It was further washed with 5 mL binding buffer and elution was
788 performed with a linear gradient of low ionic strength buffer (50 mM sodium phosphate, pH
789 7.0) for 20 × column volumes. Chromatograms for both species were exported and overlayed
790 with GraphPad Prism v. 9.5 software (GraphPad Software, San Diego, CA).

791

792 *Flow cytometry analyses*

793 - *Human endothelial cells*

794 Human skin endothelial cell line HMEC-1 (ATTC, Manassas, VA) was cultured under standard
795 conditions in a complete MCDB 131 cell culture medium (Gibco™, Thermo Fisher Scientific)
796 containing 10 % fetal calf serum (ATCC), 10 ng/mL epidermal growth factor (EGF, Thermo
797 Fisher Scientific), 1 pg/mL Hydrocortisone (Sigma-Aldrich), and 10 mM glutamine (ATCC).
798 To create pro-apoptotic conditions, HMEC-1 cells were first starved in a serum free medium
799 Opti-MEM™ (Gibco™, Thermo Fisher Scientific) for 24 hours, then they were exposed for 24
800 hours to Opti-MEM™ containing 1 mM of H_2O_2. To represent normal conditions, MCDB 131
801 medium was not changed. After incubation, the cells were washed with PBS by centrifugation
802 at 125 × g for 10 min at 4 °C. A sample of cells was stained with Trypan Blue (Gibco™, Thermo
803 Fisher Scientific) to estimate the percentage of dead cells. Following washing with PBS,
804 HMEC-1 cells were resuspended in PBS and distributed in FACS tubes with 10^5 cells per tube.
805 For assessment of cell death by flow cytometry, a part of the samples was labelled with annexin
806 V-conjugated with APC and propidium iodide (Molecular Probes, Thermo Fisher Scientific).
807 HMEC-1 cells cultured in pro-apoptotic and normal conditions were distributed and incubated
808 in the presence of Alexa Fluor™ 555-conjugated polyclonal human and bat (*M. myotis*) IgG at

809 a concentration of 25 µg/ml. To assess the effect of temperature on IgG binding to live and
810 dead cells, samples were incubated for 30 min at 22 or at 42 °C. Cells were then washed with
811 PBS at 1,600 rpm, 4°C for 10 min and binding was analyzed by flow cytometer FACS
812 LSRFortessa™ (BD Bioscience, Franklin Lakes, NJ) using Yellow/Green Ex 561 nm Em
813 586/15 laser for the detection of antibodies. Mean fluorescence intensity (MFI) indicating
814 antibody binding was measured using FlowJo Software (LLC, Ashland, OR). The data was
815 normalized by calculating the MFI ratio against the mean negative control.

816 - *Bat epithelial cells*

817 The *Myotis myotis* nasal epithelial cell line MmNep [67] was cultured in complete DMEM/F-
818 12+GlutaMAX™ (Gibco™, Thermo Fisher Scientific) containing 10 % fetal calf serum
819 (ATCC) and 1% Penicillin-Streptomycin. To create pro-apoptotic conditions, MmNep cells
820 were first starved in a serum free DMEM/F-12+GlutaMAX™ (Gibco™, Thermo Fisher
821 Scientific) for 24 hours, then they were exposed for 24 hours to DMEM/F-12+GlutaMAX™
822 containing 1 mM of H_2O_2. To represent normal conditions, DMEM/F-12+GlutaMAX™
823 medium was not changed. After incubation, the cells were detached by Trypsin 0.25%, washed
824 with PBS by centrifugation at 125 × g for 10 min at RT and resuspended in PBS. A sample of
825 cells was stained with Trypan Blue (Gibco™, Thermo Fisher Scientific) to estimate cell number
826 and condition. Following washing with PBS, MmNep cells were placed in FACS tubes with
827 3×10^5 cells per tube.

828 MmNep cells cultured in pro-apoptotic and in normal conditions were distributed and
829 incubated in the presence of Alexa Fluor™ 647-conjugated pooled bat (*M. myotis*) IgG at a
830 concentration of 25 µg/ml. To assess the effect of temperature on IgG binding to live and dead
831 cells, samples and controls were incubated for 30 min at 22 or 42 °C. Cells were then washed
832 with PBS at 125 × g, 4 °C for 10 min. For assessment of cell death by flow cytometry, control

833 samples were labelled with annexin V-conjugated with FITC and propidium iodide (Molecular
834 Probes, Thermo Fisher Scientific). Binding was analyzed by flow cytometer FACS LSR 2 (BD
835 Bioscience, Franklin Lakes, NJ) using Red 660/20 for the detection of antibodies. Mean
836 fluorescence intensity (MFI) indicating antibody binding was measured using FlowJo Software
837 (LLC, Ashland, OR).

838

839 *Bioinformatics analyses*

840 Sequences of *M. lucifugus* variable regions (VH3) were retrieved from the literature[30].
841 Sequences of human variable regions (VH3) from naïve and IgM memory B cells were
842 obtained from following study [69]. Framework (FR) and Complementarity-Determining (CDR)
843 regions were delineated based on IMGT unique numbering [70]. Of note, the three first amino
844 acids at the N-terminal extremity of the FRH1 were not provided for the bat sequences.
845 Accordingly, these residues were also removed from the analysis of human sequences. GRAVY
846 index was computed with Gravy Calculator (https://www.gravy-calculator.de). Amino acid
847 counts were done with Microsoft Excel (version 2018). Statistical analysis was performed with
848 GraphPad Prism v. 9.5 software.

849 Sequences of bat constant region were obtained from NCBI Genome Data Viewer [71] selecting
850 *Myotis myotis* organism and searching for loci annotated as "immunoglobulin heavy constant
851 gamma". Among the three hits, we selected those localized on NW_023416326.1 and
852 NW_023416348.1 (the sequence of the third hit is identical to the sequence on
853 NW_023416326.1). Human and mouse reference sequences for the constant region of heavy
854 chains were obtained from IMGT/GENE-DB [72]. Sequence alignments, phylogenetic trees, and
855 percent of identity were obtained with Clustal Omega [73].

856

857 **References**

858 1 Gorbunova, V., Seluanov, A. & Kennedy, B. K. The World Goes Bats: Living Longer
859 and Tolerating Viruses. *Cell Metab* **32**, 31-43 (2020).
860 2 Smith, I. & Wang, L. F. Bats and their virome: an important source of emerging viruses
861 capable of infecting humans. *Curr Opin Virol* **3**, 84-91 (2013).
862 3 Luis, A. D. *et al.* A comparison of bats and rodents as reservoirs of zoonotic viruses:
863 are bats special? *Proc Biol Sci* **280**, 20122753 (2013).
864 4 Chan, J. F., To, K. K., Tse, H., Jin, D. Y. & Yuen, K. Y. Interspecies transmission and
865 emergence of novel viruses: lessons from bats and birds. *Trends Microbiol* **21**, 544-555
866 (2013).
867 5 Olival, K. J. *et al.* Host and viral traits predict zoonotic spillover from mammals. *Nature*
868 **546**, 646-650 (2017).
869 6 Holmes, E. C. The Ecology of Viral Emergence. *Annu Rev Virol* **9**, 173-192 (2022).
870 7 Letko, M., Seifert, S. N., Olival, K. J., Plowright, R. K. & Munster, V. J. Bat-borne
871 virus diversity, spillover and emergence. *Nat Rev Microbiol* **18**, 461-471 (2020).
872 8 Banerjee, A. *et al.* Novel Insights Into Immune Systems of Bats. *Front Immunol* **11**, 26
873 (2020).
874 9 Irving, A. T., Ahn, M., Goh, G., Anderson, D. E. & Wang, L. F. Lessons from the host
875 defences of bats, a unique viral reservoir. *Nature* **589**, 363-370 (2021).
876 10 Zhou, P. *et al.* Contraction of the type I IFN locus and unusual constitutive expression
877 of IFN-alpha in bats. *Proc Natl Acad Sci U S A* **113**, 2696-2701 (2016).
878 11 Clayton, E. & Munir, M. Fundamental Characteristics of Bat Interferon Systems. *Front*
879 *Cell Infect Microbiol* **10**, 527921 (2020).
880 12 Ahn, M., Cui, J., Irving, A. T. & Wang, L. F. Unique Loss of the PYHIN Gene Family
881 in Bats Amongst Mammals: Implications for Inflammasome Sensing. *Sci Rep* **6**, 21722
882 (2016).
883 13 Xie, J. *et al.* Dampened STING-Dependent Interferon Activation in Bats. *Cell Host*
884 *Microbe* **23**, 297-301 e294 (2018).
885 14 Ahn, M. *et al.* Dampened NLRP3-mediated inflammation in bats and implications for
886 a special viral reservoir host. *Nat Microbiol* **4**, 789-799 (2019).
887 15 Goh, G. *et al.* Complementary regulation of caspase-1 and IL-1beta reveals additional
888 mechanisms of dampened inflammation in bats. *Proc Natl Acad Sci U S A* **117**, 28939-
889 28949 (2020).
890 16 O'Shea, T. J. *et al.* Bat flight and zoonotic viruses. *Emerg Infect Dis* **20**, 741-745 (2014).
891 17 Fumagalli, M. R., Zapperi, S. & La Porta, C. A. M. Role of body temperature variations
892 in bat immune response to viral infections. *J R Soc Interface* **18**, 20210211 (2021).
893 18 Halsall, A. L., Boyles, J. G. & Whitaker Jr, J. O. Body temperature patterns of big brown
894 bats during winter in a building hibernaculum. *Journal of Mammalogy* **93**, 497-503
895 (2012).
896 19 Mayberry, H. W., McGuire, L. P. & Willis, C. K. R. Body temperatures of hibernating
897 little brown bats reveal pronounced behavioural activity during deep torpor and suggest
898 a fever response during white-nose syndrome. *J Comp Physiol B* **188**, 333-343 (2018).
899 20 Evans, S. S., Repasky, E. A. & Fisher, D. T. Fever and the thermal regulation of
900 immunity: the immune system feels the heat. *Nat Rev Immunol* **15**, 335-349 (2015).
901 21 Lu, L. L., Suscovich, T. J., Fortune, S. M. & Alter, G. Beyond binding: antibody effector
902 functions in infectious diseases. *Nat Rev Immunol* **18**, 46-61 (2018).
903 22 Thomas, S. & Suthers, R. A. The physiology and energetics of bat flight. *J. Exp. Biol.*
904 **57**, 317-335 (1972).

23 Park, K. J., Jones, G. & Ransome, R. D. Torpor, arousal and activity of hibernating Greater Horseshoe Bats (Rhinolophus ferrumequinum). *Funct. Ecol.* **14**, 580-588 (2000).
24 Geiser, F. Metabolic rate and body temperature reduction during hibernation and daily torpor. *Annu Rev Physiol* **66**, 239-274 (2004).
25 Geiser, F. & Stawski, C. Hibernation and torpor in tropical and subtropical bats in relation to energetics, extinctions, and the evolution of endothermy. *Integr Comp Biol* **51**, 337-348 (2011).
26 Luo, J. *et al.* Flight rapidly modulates body temperature in freely behaving bats. *Anim Biotelemetry* **9**, 45-54 (2021).
27 Lewden, A., Bishop, C. M. & Askew, G. N. How birds dissipate heat before, during and after flight. *J R Soc Interface* **20**, 20230442 (2023).
28 Bouma, H. R., Carey, H. V. & Kroese, F. G. Hibernation: the immune system at rest? *J Leukoc Biol* **88**, 619-624 (2010).
29 Toshkova, N., Zhelyazkova, V., Justesen, S. & Dimitrov, J. D. Conservative pattern of interaction of bat and human IgG antibodies with FcRn. *Dev Comp Immunol* **139**, 104579 (2023).
30 Bratsch, S., Wertz, N., Chaloner, K., Kunz, T. H. & Butler, J. E. The little brown bat, M. lucifugus, displays a highly diverse V H, D H and J H repertoire but little evidence of somatic hypermutation. *Dev Comp Immunol* **35**, 421-430 (2011).
31 Labrousse, H., Adib-Conquy, M. & Avrameas, S. Effect of temperature on the reactivities of polyreactive and monospecific monoclonal IgG antibodies. *Res Immunol* **148**, 267-276 (1997).
32 Ditzel, H. J., Itoh, K. & Burton, D. R. Determinants of polyreactivity in a large panel of recombinant human antibodies from HIV-1 infection. *J Immunol* **157**, 739-749 (1996).
33 Ortega, E., Kostovetzky, M. & Larralde, C. Natural DNP-binding immunoglobulins and antibody multispecificity. *Mol Immunol* **21**, 883-888 (1984).
34 Gunti, S. & Notkins, A. L. Polyreactive Antibodies: Function and Quantification. *J Infect Dis* **212 Suppl 1**, S42-46 (2015).
35 Labrousse, H., Adib-Conquy, M. & Avrameas, S. Effects of pH or ionic strength on the reactivities of mono- and polyspecific IgG antibodies. *Res Immunol* **145**, 541-552 (1994).
36 Tokuriki, N. & Tawfik, D. S. Stability effects of mutations and protein evolvability. *Curr Opin Struct Biol* **19**, 596-604 (2009).
37 Teilum, K., Olsen, J. G. & Kragelund, B. B. Protein stability, flexibility and function. *Biochim Biophys Acta* **1814**, 969-976 (2011).
38 Manivel, V., Sahoo, N. C., Salunke, D. M. & Rao, K. V. Maturation of an antibody response is governed by modulations in flexibility of the antigen-combining site. *Immunity* **13**, 611-620 (2000).
39 James, L. C., Roversi, P. & Tawfik, D. S. Antibody multispecificity mediated by conformational diversity. *Science* **299**, 1362-1367 (2003).
40 Guthmiller, J. J. *et al.* Polyreactive Broadly Neutralizing B cells Are Selected to Provide Defense against Pandemic Threat Influenza Viruses *Immunity* **53**, 1230-1244.e1235 (2020).
41 Klein, F. *et al.* Somatic mutations of the immunoglobulin framework are generally required for broad and potent HIV-1 neutralization. *Cell* **153**, 126-138 (2013).
42 Schellman, J. A. Temperature, stability, and the hydrophobic interaction. *Biophys J* **73**, 2960-2964 (1997).

43 Chandler, D. Interfaces and the driving force of hydrophobic assembly. *Nature* **437**, 640-647 (2005).
44 Baker, M. L., Tachedjian, M. & Wang, L. F. Immunoglobulin heavy chain diversity in Pteropid bats: evidence for a diverse and highly specific antigen binding repertoire. *Immunogenetics* **62**, 173-184 (2010).
45 Butler, J. E. *et al.* The two suborders of chiropterans have the canonical heavy-chain immunoglobulin (Ig) gene repertoire of eutherian mammals. *Dev Comp Immunol* **35**, 273-284 (2011).
46 Larson, P. A. *et al.* Genomic features of humoral immunity support tolerance model in Egyptian rousette bats. *Cell Rep* **35**, 109140 (2021).
47 Stawski, C., Willis, C. K. & Geiser, F. The importance of temporal heterothermy in bats. *Journal of Zoology* **292**, 86-100 (2014).
48 Ruf, T. & Geiser, F. Daily torpor and hibernation in birds and mammals. *Biol Rev Camb Philos Soc* **90**, 891-926 (2015).
49 Canale, C. I. & Henry, P. Y. Energetic costs of the immune response and torpor use in a primate. *Funct. Ecol.* **25**, 557-565 (2011).
50 Ganeshan, K. *et al.* Energetic Trade-Offs and Hypometabolic States Promote Disease Tolerance. *Cell* **177**, 399-413 e312 (2019).
51 Drexler, J. F. *et al.* Bats host major mammalian paramyxoviruses. *Nat Commun* **3**, 796 (2012).
52 Schatz, J. *et al.* Enhanced passive bat rabies surveillance in indigenous bat species from Germany--a retrospective study. *PLoS Negl Trop Dis* **8**, e2835 (2014).
53 Fagre, A. C. & Kading, R. C. Can Bats Serve as Reservoirs for Arboviruses? *Viruses* **11** (2019).
54 Kim, Y. *et al.* Transmission dynamics of lyssavirus in Myotis myotis: mechanistic modelling study based on longitudinal seroprevalence data. *Proc Biol Sci* **290**, 20230183 (2023).
55 Zhang, G. *et al.* Comparative analysis of bat genomes provides insight into the evolution of flight and immunity. *Science* **339**, 456-460 (2013).
56 Jebb, D. *et al.* Six reference-quality genomes reveal evolution of bat adaptations. *Nature* **583**, 578-584 (2020).
57 Costantini, D., Lindecke, O., Petersons, G. & Voigt, C. C. Migratory flight imposes oxidative stress in bats. *Curr Zool* **65**, 147-153 (2019).
58 Shen, Y. Y. *et al.* Adaptive evolution of energy metabolism genes and the origin of flight in bats. *Proc Natl Acad Sci U S A* **107**, 8666-8671 (2010).
59 Gonzalez, V. & Banerjee, A. Molecular, ecological, and behavioral drivers of the bat-virus relationship. *iScience* **25**, 104779 (2022).
60 Chang, M. K. *et al.* Apoptotic cells with oxidation-specific epitopes are immunogenic and proinflammatory. *J Exp Med* **200**, 1359-1370 (2004).
61 Poon, I. K., Hulett, M. D. & Parish, C. R. Molecular mechanisms of late apoptotic/necrotic cell clearance. *Cell Death Differ* **17**, 381-397 (2010).
62 Poon, I. K., Lucas, C. D., Rossi, A. G. & Ravichandran, K. S. Apoptotic cell clearance: basic biology and therapeutic potential. *Nat Rev Immunol* **14**, 166-180 (2014).
63 Chou, M. Y. *et al.* Oxidation-specific epitopes are dominant targets of innate natural antibodies in mice and humans. *J Clin Invest* **119**, 1335-1349 (2009).
64 Zhou, Z. H. *et al.* Polyreactive antibodies plus complement enhance the phagocytosis of cells made apoptotic by UV-light or HIV. *Sci Rep* **3**, 2271 (2013).
65 Silverman, G. J. Protective natural autoantibodies to apoptotic cells: evidence of convergent selection of recurrent innate-like clones. *Ann N Y Acad Sci* **1362**, 164-175 (2015).

66 Wimsatt, J., O'Shea, T. J., Ellison, L. E., Pearce, R. D. & Price, V. R. Anesthesia and blood sampling of wild big brown bats (eptesicus fuscus) with an assessment of impacts on survival. *J Wildl Dis* **41**, 87-95 (2005).
67 He, X. *et al.* Establishment of Myotis myotis cell lines--model for investigation of host-pathogen interaction in a natural host for emerging viruses. *PLoS One* **9**, e109795 (2014).
68 Bozinovic, N., Noe, R., Kanyavuz, A., Lecerf, M. & Dimitrov, J. D. Method for identification of heme-binding proteins and quantification of their interactions. *Anal Biochem* **607**, 113865 (2020).
69 Shehata, L. *et al.* Affinity Maturation Enhances Antibody Specificity but Compromises Conformational Stability. *Cell Rep* **28**, 3300-3308 e3304 (2019).
70 Lefranc, M. P. IMGT unique numbering for the variable (V), constant (C), and groove (G) domains of IG, TR, MH, IgSF, and MhSF. *Cold Spring Harb Protoc* **2011**, 633-642 (2011).
71 Rangwala, S. H. *et al.* Accessing NCBI data using the NCBI Sequence Viewer and Genome Data Viewer (GDV). *Genome Res* **31**, 159-169 (2021).
72 Giudicelli, V., Chaume, D. & Lefranc, M. P. IMGT/GENE-DB: a comprehensive database for human and mouse immunoglobulin and T cell receptor genes. *Nucleic Acids Res* **33**, D256-261 (2005).
73 Madeira, F. *et al.* Search and sequence analysis tools services from EMBL-EBI in 2022. *Nucleic Acids Res* **50**, W276-W279 (2022).

Acknowledgments

The experimental work was supported by a grant from European Research Council (Project CoBABATI ERC-StG-678905), awarded to J.D.D. Fieldwork funding was provided by the Bulgarian National Science Fund (project KP-06-N51/9 “Caves as a reservoir for novel and reoccurring zoonoses - ecological monitoring and metagenomic analysis in real-time”). NT was funded by a Ph.D. Fellowship from Karoll Knowledge Foundation and a stipend from the French Institute, Bulgaria. VZ was supported by a stipend from the French Institute, Bulgaria.

We would like to express our gratitude to the volunteers who assisted us in the field: Boris Petrov, Petar Velkov, Katrin Dimitrova, Kaloyana Koseva, Kristin Meshinska, and Stela-Teodora Trendafilova. Our heartfelt thanks go to Dr Lubka Roumenina, and Dr Sebastien Lacroix-Desmazes (both from Centre de Recherche des Cordeliers, Paris, France) for their

insightful feedback on our ideas and their unwavering intellectual support throughout this study. We thank Dr Hugo Mouquet, Dr Vishu Kumar Aimanianda (both from Institute Pasteur, Paris, France) and Dr Stephane Mesnage, (University of Sheffield, UK) for providing us with some important material (pathogen proteins, antibodies, and plasmids). We also thank Pr. J. Pikula and Dr. V. Kovácová (Department of Ecology and Diseases of Zoo Animals, Game, Fish and Bees, University of Veterinary and Pharmaceutical Sciences Brno) for sharing the MmNep cells.

Author contributions

N.T., V.Z., and J.D.D. conceived the study; N.T., V.Z., N.J., C.P., and J.D.D., designed the experiments; N.T., and V.Z. collected essential samples; N.J. and G.G. provided essential samples and materials; N.T., V.Z., A.R.R., E.H., M.C.D., R.V.L., M.L. and J.D.D. performed the experiments. N.T., V.Z., A.R.R., E.H., R.V.L., M.L., and J.D.D. analyzed the obtained data; J.D.D. supervised the research; J.D.D. wrote the manuscript; all authors contributed to editing of the manuscript.

Competing interests

The authors declare no competing interests.

Data availability

All raw data supporting the findings of this study are available upon request from the corresponding author.

1063

1064 **Figure Legends**

1065 **Figure 1.** Temperature modulates antigen binding properties of bat IgG. **a.** Heat map depicting
1066 binding intensity of IgG purified from pooled sera of *N. noctula, M. myotis*, and healthy human
1067 (two different pools) to a panel of antigens. The IgG were purified from sera pools with 4-5
1068 individuals. Reactivity of bat and human IgG was evaluated at 4, 22 and 42 °C by ELISA.
1069 Binding of IgG to the blocking agent (Bckg) is also shown. Binding intensity against each
1070 target represent average optical density (n=2 for *M. Myotis* and human; and n=2 and n=1 for
1071 *N. noctula*) after subtraction of the background binding (measured after incubation of the
1072 detection reagents with the respective antigens in the absence of antibodies). Violin plots
1073 corresponding to each heat map show the Z-score values of antigen binding. The Z-score for
1074 each target antigen is presented as an individual circle. *P* values were determined using one-
1075 way analysis of variance (ANOVA) with Friedman multiple comparison test, $*p < 0.05$,
1076 $***p < 0.001$, n.s., not significant. **b.** Real-time interaction profiles showing binding of *M.*
1077 *myotis* IgG to Rabies virus glycoprotein and TBEV NS1 immobilized on a sensor chip as a
1078 function of temperature. Antibodies were injected at serial dilutions at a concentration range
1079 670 – 41.875 nM. Apparent binding affinities were evaluated by global kinetic analyses based
1080 on results obtained at 40 °C. Kinetic fits of the same analyses are presented in **Supplementary**
1081 **Fig. 4**. **c**. Effect of temperature on antigen binding by bat and human IgG in whole sera. Pooled
1082 bat and human sera were serially diluted from 60 × to 1920 × and incubated with immobilized
1083 antigens at 4, 22 and 42 °C. Each data point represents average IgG binding intensity ±SD from
1084 n=3 technical replicates. **d**. Immunofluorescence analyses of bat and human IgG binding to
1085 HEp-2 cells at 22 and 42 °C. The images are representative examples from n=9 fluorescence
1086 acquisitions from two independent experiments (magnification × 63). **e**. Quantification of
1087 fluorescence intensity from immunofluorescence analyses of binding of bat and human IgG to
1088 Hep-2 cells. The graphs show the mean fluorescence intensity of n=9 images, for each
1089 condition, acquired in two independent experiments. Statistical analyses were performed by a
1090 nonparametric t-test, Mann-Whitney test, $****p < 0.0001$. The white bar corresponds to 10
1091 μm.

1092

1093 **Figure 2.** Bat antibodies acquire broad reactivity towards diverse proteins at elevated
1094 temperature. Presented plots depict summarized results from protein microarray analyses of
1095 binding of bat (*M. myotis*) and human pooled IgG to > 17 000 human proteins. **a**. Antibody
1096 reactivity at 22 °C was plotted versus reactivity at 42 °C; **b**. Reactivities of bat versus human
1097 IgG. Each dot in a and b represent the average MFI (n=2) signifying IgG binding to a single
1098 protein in the array, after subtraction of the background reactivity. Red dashed lines represent
1099 the threshold of 1000 MFI, identifying antibody specificities with high binding intensity. **c.** Z-
1100 scores of antibody binding reactivities to human proteins. Each dot represents the Z-score
1101 characterizing binding reactivity to a single protein. The threshold indicated with red dotted
1102 lines corresponds to Z=2 and $p < 0.05$.

1103

1104 **Figure 3**. Temperature sensitivity of bat IgG is mediated by Fab. **a.** A schematic representation
1105 of the experimental procedure for the generation of $F(ab')_2$ fragments from IgG of *M. myotis*.
1106 **b.** Reactivity of bat $F(ab')_2$ to a panel of antigens as a function of temperature. Binding intensity
1107 values were obtained after incubation of 10 μg/ml (67 nM) of $F(ab')_2$ fragments with a panel
1108 of immobilized antigens at 4 °C (blue), 22 °C (orange), and 42 °C (red). Each point corresponds
1109 to an individual technical replicate for each condition after subtraction of the background
1110 (obtained following incubation of the detection reagents with the respective antigens in the
1111 absence of $F(ab')_2$ fragments). Control reactivity of bat $F(ab')_2$ to the surface in the absence of
1112 antigens is also shown. **c.** A schematic representation of the experimental setting for the
1113 evaluation of interactions of C1q, FcRn, and protein G with the Fc-fragment of bat IgG. **d.**
1114 Real-time interaction profiles of binding of human C1q (0.625 nM) with immobilized IgG from
1115 *M. myotis*, *N. noctula* and human. Binding curves obtained at 4 °C (blue), 22 °C (orange), and
1116 40 °C (red) are depicted. Real-time interaction curves were obtained after subtraction of C1q
1117 binding to a control surface without immobilized IgG. **e.** Real-time interaction profiles showing
1118 binding of human recombinant FcRn to IgG from *M. myotis*, *N. noctula* and human
1119 immobilized on sensor chip. FcRn was injected at serial dilutions in concentration range 25 -
1120 0.097 nM (2 × dilution step) in a buffer with pH 5.7. **f.** Real-time interaction profiles showing
1121 binding of recombinant protein G to IgG from *M. myotis*, *N. noctula,* and human immobilized
1122 on sensor chip. Protein G was injected at serial dilutions in concentration range 100 – 0.046
1123 nM (3 × dilution step). For **e.** and **f.** Measurements were performed at 22 °C and 40 °C. The
1124 values of equilibrium association constants (shown in plots on the right) were evaluated by

1125 global Langmuir kinetics analyses model. The real-time binding profiles after subtraction of
1126 reactivity to a control surface are shown by black lines. The global kinetic fit is depicted by red
1127 lines. For e. representative results from two independent experiments is shown.

1128

1129 **Figure 4.** Bat IgG is characterized by untypical physiochemical characteristics. **a.** Melting
1130 temperatures of bat (*M. myotis*) and human IgG, obtained by thermal-shift assay. Each dot
1131 indicates an individual estimation of the melting temperature. The results of two independent
1132 experiments are presented together. Statistical significance was assessed by applying a
1133 nonparametric t-test analysis, Mann-Whitney test. $^{**}p = 0.0022$. A comparison of the
1134 thermodynamic stability of IgG from another bat species (*M. capaccinii*) with the stability of
1135 human IgG is depicted in Supplementary Fig. 11. **b**. Overall hydrophobicity of human and bat
1136 IgG. Elution profiles of polyclonal human and *M. myotis* IgG (green and purple lines,
1137 respectively) obtained by hydrophobic interaction chromatography. Chromatography profiles
1138 were obtained by measuring protein absorbance changes at 280 nm. The normalized profiles
1139 are presented. The brown dotted line depicts the elution gradient of buffer with a decreasing
1140 ionic strength as assessed by changes in conductivity. A representative result from two
1141 independent experiments is shown. **c.** Ionic strength dependence of antigen binding of bat and
1142 human IgG. Polyclonal IgG from *M. myotis* (purple symbols and line), *N. noctula* (red symbols
1143 and line), and human (green symbols and line) were diluted to 20 μg/ml in 10 mM HEPES
1144 buffer containing increasing concentrations of NaCl: 0, 0.0078, 0.0156, 0.0312, 0.0625, 0.125,
1145 0.25, 0.5, 1, 2 and 4M and incubated with the indicated proteins immobilized on ELISA plate.
1146 Each data point represents average optical density (n=2) ±SD. **d.** *In silico* comparison of the
1147 hydrophobicity of the variable region of human and *Myotis lucifugus* heavy immunoglobulin
1148 chains. The hydrophobicity index was calculated by GRAVY calculator (https://www.gravy-
1149 calculator.de) (in bulk or by subregions) using amino acid sequences taken from [30] (*M.*
1150 *lucifugus*) and [69] (human). Statistical analyses were performed by using Two-way ANOVA,
1151 with Šídák's multiple comparisons test, $^{**}p < 0.01$, $^{***}p < 0.001$.

1152

1153 **Figure 5.** Bat antibody repertoires have higher level of polyreactive IgG antibodies. **a.** Heat
1154 maps depicting binding intensity of human polyreactive (ED38) and monoreactive (VRC01
1155 and S309) IgG1 to a set of distinct antigens. Reactivity of monoclonal antibodies was evaluated
1156 at 4, 22 and 42 °C by ELISA. Binding of IgG to the blocking agent (Bckg) is also shown.

1157 Binding intensity against each target represent average optical density (n=2) after subtraction
1158 of the background binding measured after incubation of the detection reagents with the
1159 respective antigens in absence of IgG. For the analyses, all antibodies were diluted to 10 μg/ml.
1160 Violin plots corresponding to each heat map show the Z-score values of antigen binding. The
1161 Z-score for each target antigen is presented as an individual circle. *P* values were determined
1162 using one-way analysis of variance (ANOVA) with Friedman multiple comparison test, **p* =
1163 0.0153, ***p* = 0.0035, n.s., not significant. **b.** and **c.** Binding of increasing concentrations of
1164 human and bat (*M. myotis* and *N. noctula*) IgG antibodies (b) and human monoclonal IgG1
1165 antibodies (c) to immobilized DNP-BSA. Each data point on the graphs represents average
1166 optical density (n=3) ±SD. Representative results from two independent experiments are
1167 shown. **d.** Immunoblot analyses of bat IgG binding to lysate of bat epithelial cells. The figure
1168 shows the reactivity of increasing concentrations (2.5 - 20 μg/ml) of IgG from *M. myotis* and
1169 *N. noctula* towards proteins from crude extract of MmNep epithelial cells from *M. myotis*. The
1170 antibodies were alternatively diluted in buffer (PBS) with physiological and low ionic strength.
1171 A representative example from two independent experiments is shown. **e.** Immunofluorescence
1172 analyses of binding of *M. myotis* IgG to MmNep cells at 22 and 42 °C. The images are
1173 representative examples from n=12 fluorescence acquisitions from one of two independent
1174 experiments (magnification × 63). The white bar corresponds to 10 μm. **f.** Quantification of
1175 fluorescence intensity from immunofluorescence analyses of bat IgG binding to MmNep cells.
1176 The graph shows the mean fluorescence intensity of n=12 images. Statistical analyses were
1177 performed using Two-way ANOVA multiple comparison test, ****p < 0.0001.

1178

1179 **Figure 6.** Temperature triggers preferential binding of bat antibodies to dead endothelial cells.
1180 **a**. Gating strategy and identification of cell death induction in HMEC-1 cells by oxidative
1181 stress. Dead cells are defined as double positive for annexin V and propidium iodide. **b**. Binding
1182 of bat (*M. myotis*) and human pooled IgG to alive and dead HMEC-1 cells as a function of
1183 temperature. Representative histograms from two independent experiments show binding of
1184 fluorochrome labeled (Alexa Fluor™ 555) pooled IgG at 25 μg/ml at 22 and 42 °C. **c**.
1185 Quantification of bat and human IgG binding to alive and dead HMEC-1 cells. The average
1186 binding ± SD depicting the reactivity of antibodies was calculated from sample replicates (n=2-
1187 4) of mean fluorescence intensity (MFI). Each circle in the graph represents an MFI value.
1188 Statistical significance was evaluated by applying Two-way ANOVA Tukey's multiple
1189 comparison test. *****p* < 0.0001.

1190

1191 **Figure 7.** Temperature triggers preferential binding of bat antibodies to dead bat epithelial
1192 cells. **a**. Gating strategy and identification of cell death induction in *M. myotis* epithelial cells
1193 (MmNep) by oxidative stress. Dead cells are defined as double positive for annexin V and
1194 propidium iodide. **b**. Binding of bat (*M. myotis*) IgG to alive and dead MmNep cells as a
1195 function of temperature. Representative histograms from four independent experiments shown
1196 binding of fluorochrome labeled (Alexa Fluor™ 647) pooled IgG from *M. myotis* at 25 μg/ml
1197 at 22 and 42 °C. **c**. Quantification of bat IgG binding to alive and dead bat epithelial cells. The
1198 average binding ± SD depicting the reactivity of antibodies was calculated from sample
1199 replicates (n=6-9) of mean fluorescence intensity (MFI) obtained in three independent
1200 experiments. Each circle in the graph represents an MFI value. Statistical significance was
1201 evaluated by applying Two-way ANOVA Tukey's multiple comparison test. ****$p < 0.0001$.

1202

1203

1204

1205

1206

1207

1208

1209

1210

1211

1212

1213

1214

1215

1216

1217

1218 **Figure 1**

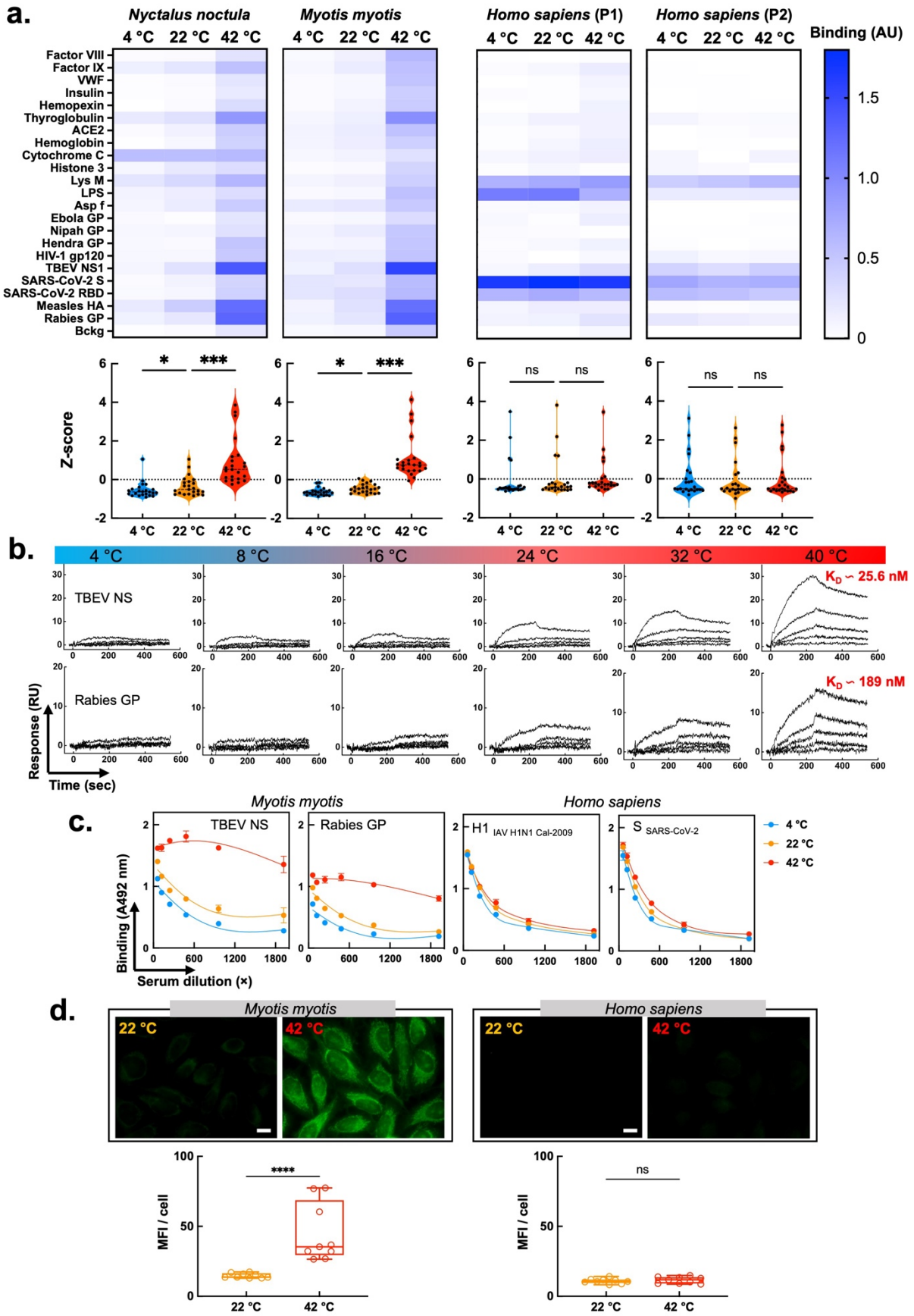

1219

1220 **Figure 2**

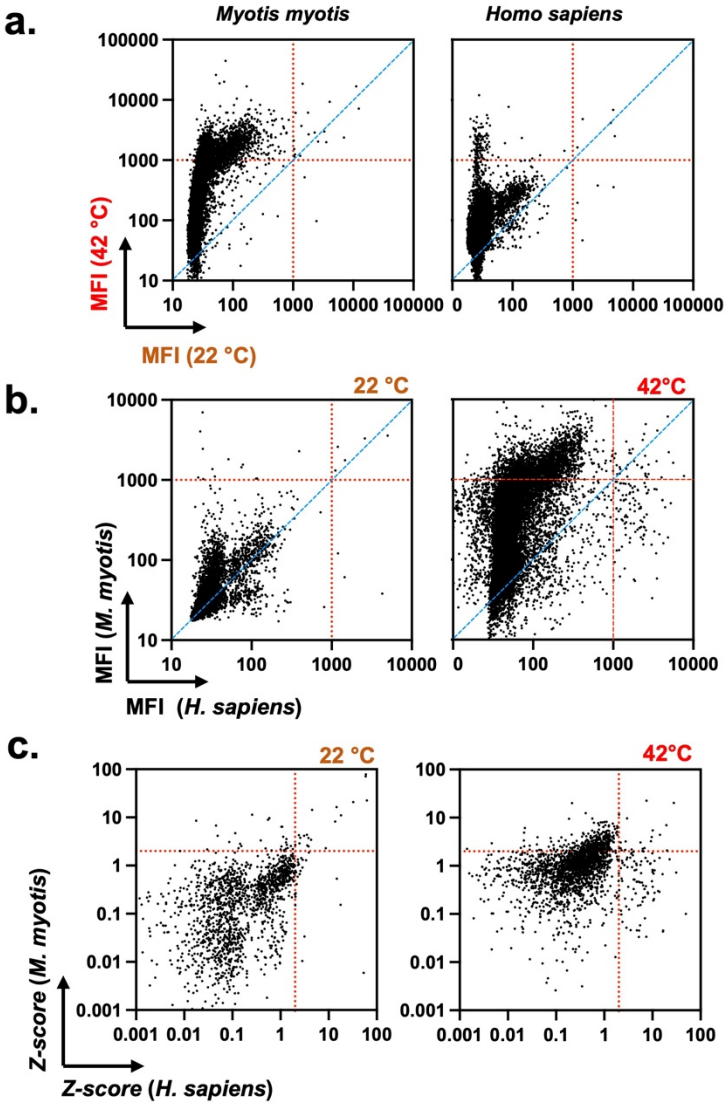

1221

1222 **Figure 3**

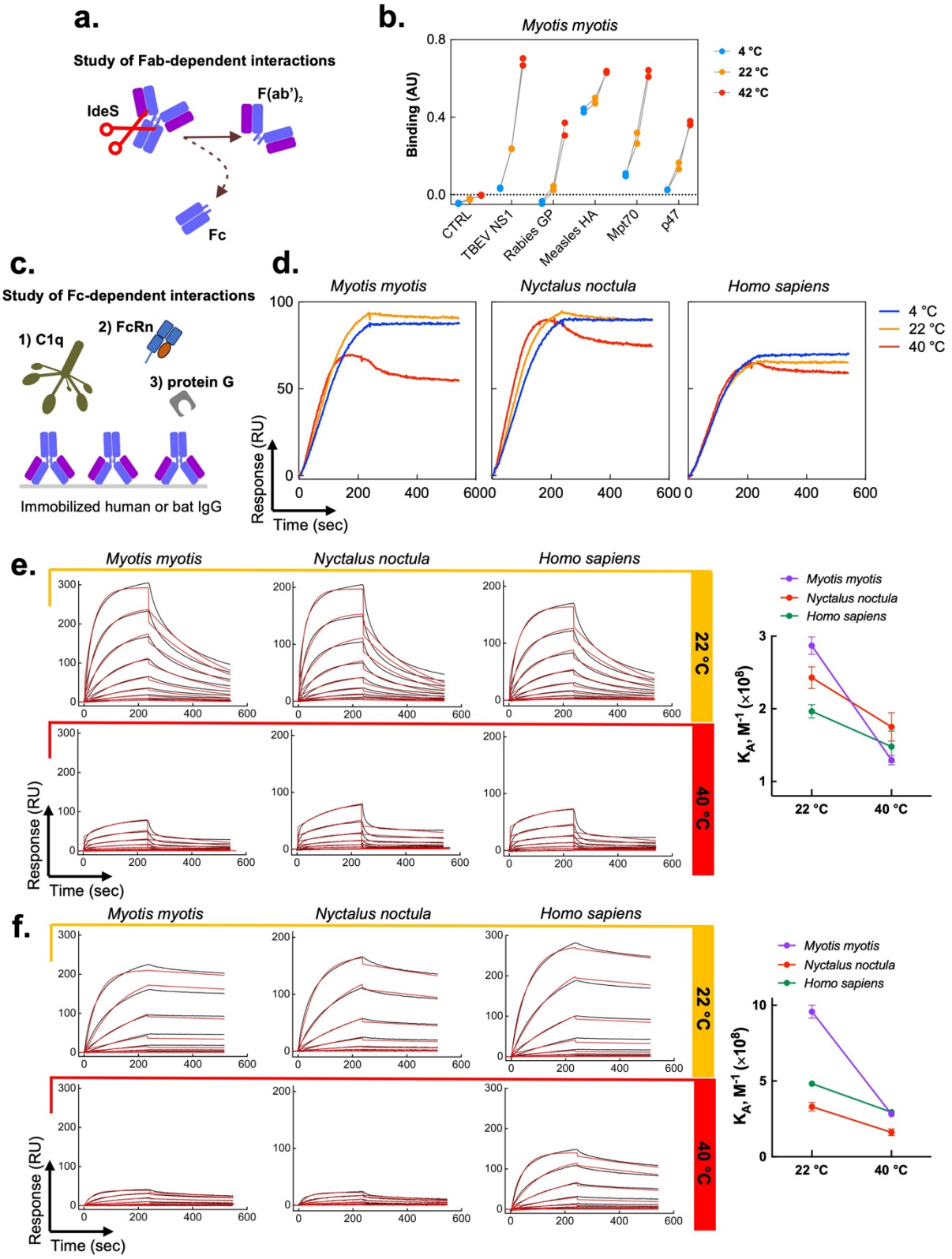

1223

1224 **Figure 4**

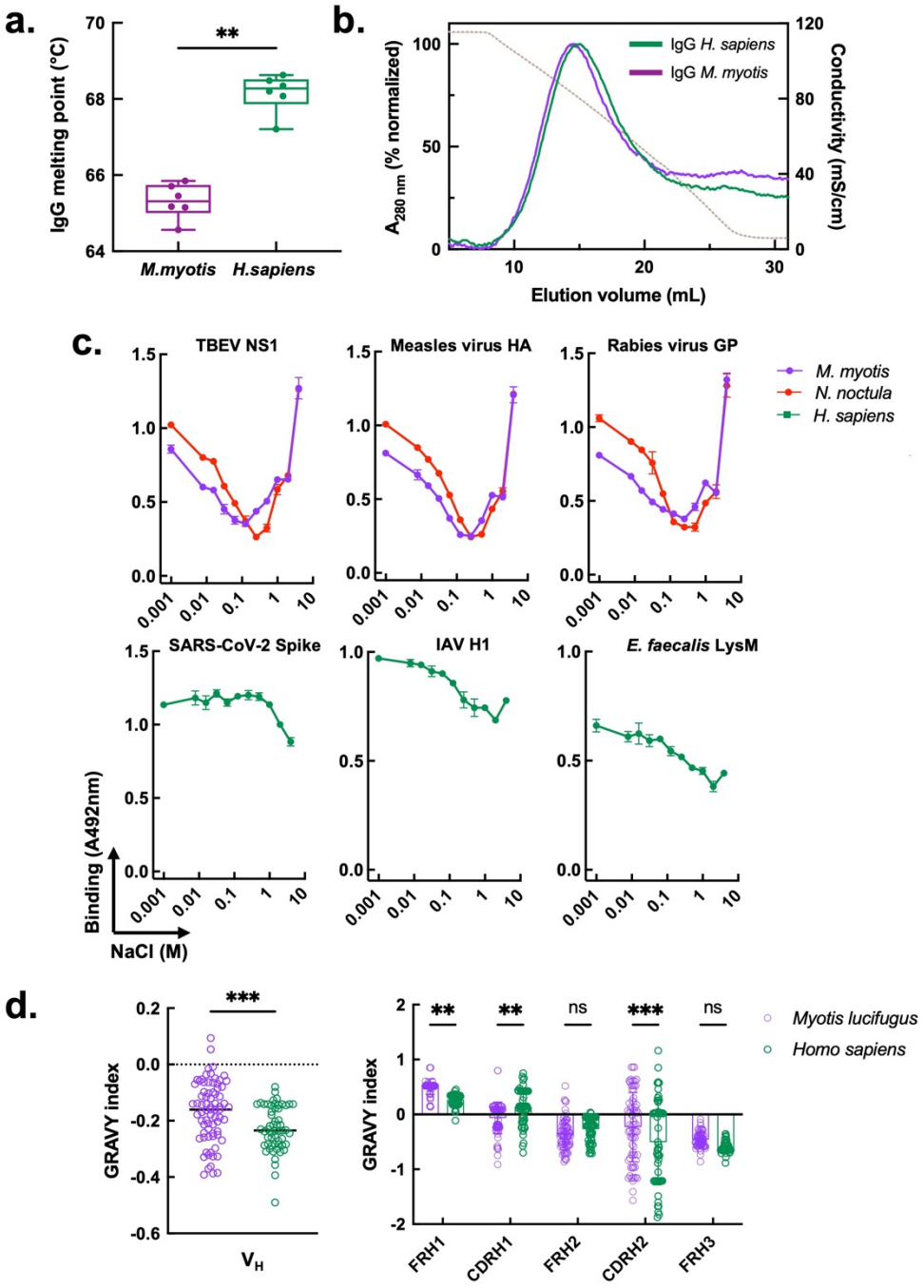

1225

1226 **Figure 5**

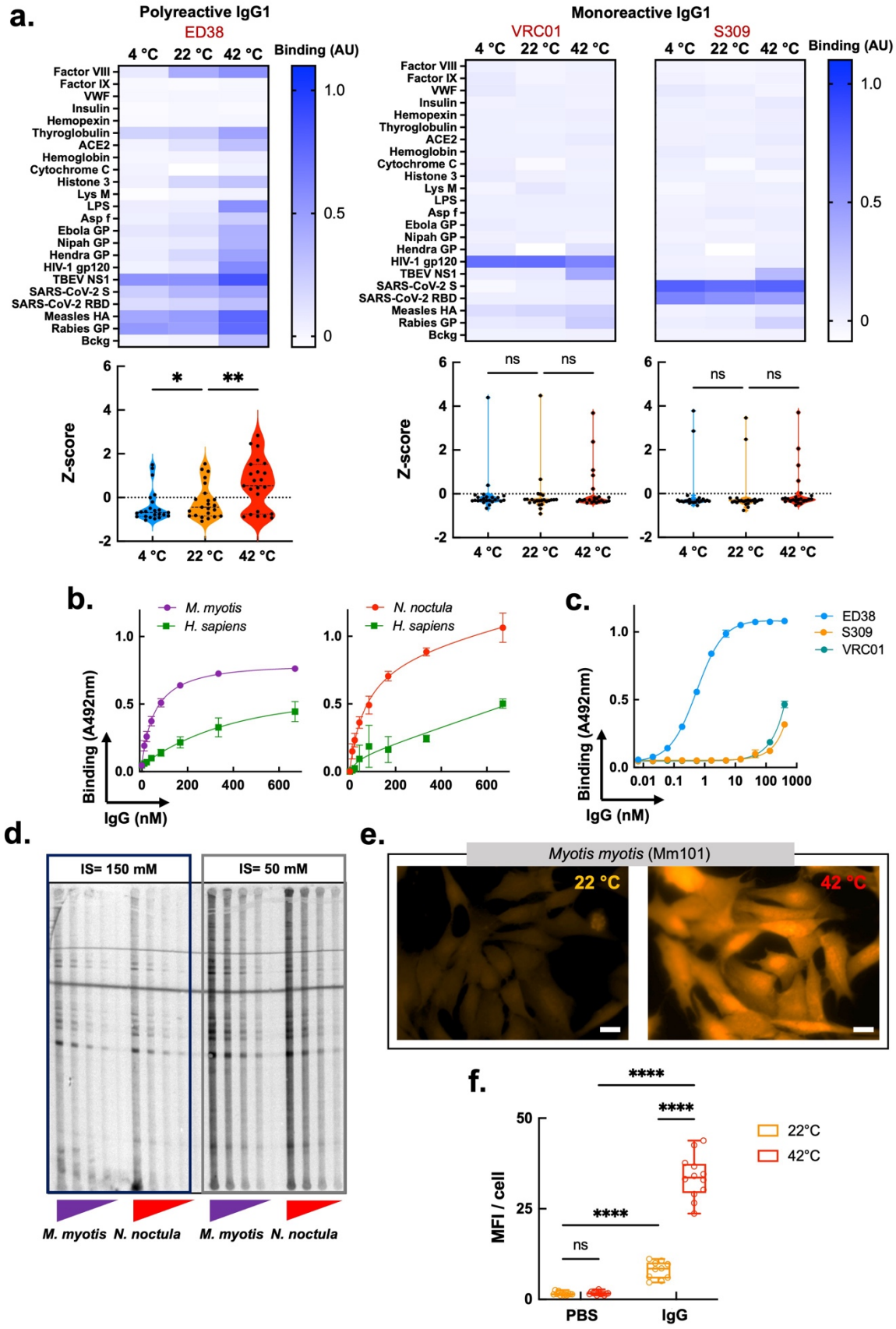

1227

1228 **Figure 6**

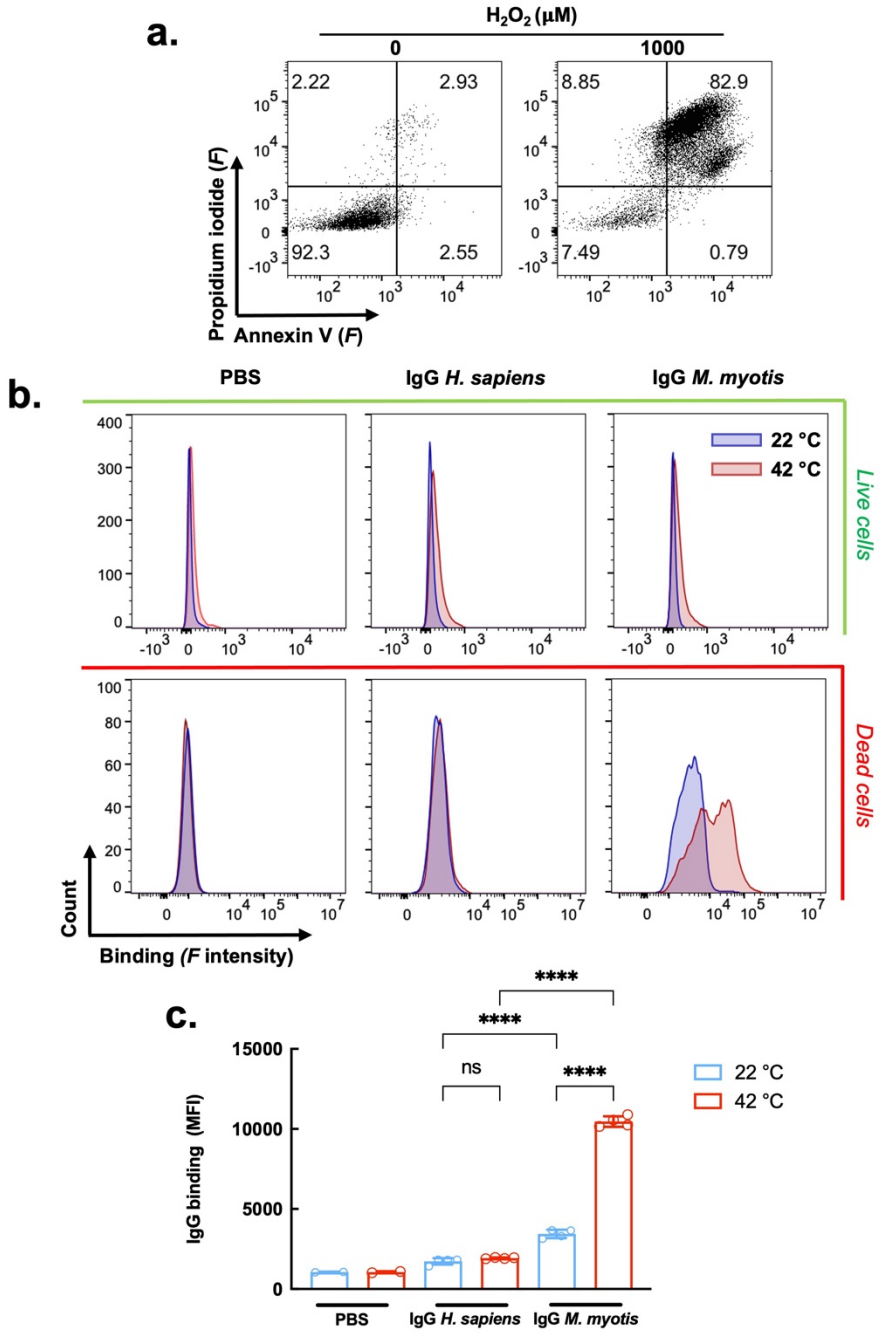

1229

1230 **Figure 7**

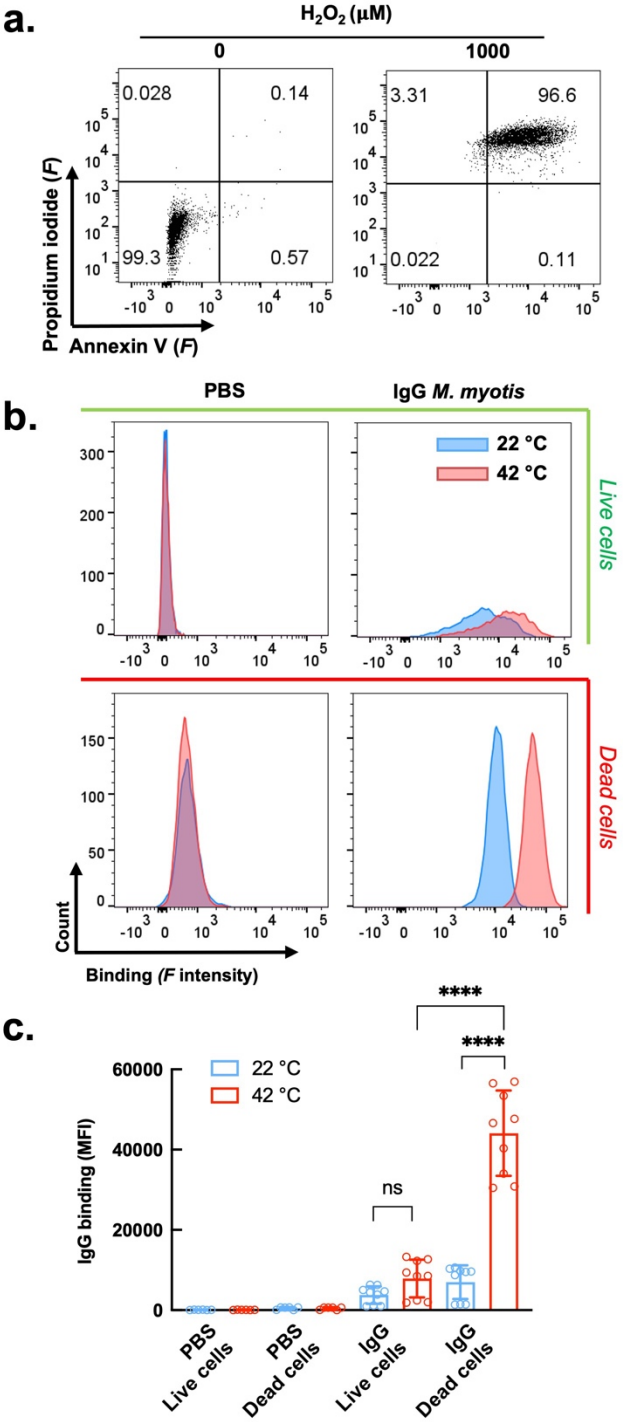

1231